MSC-04112
Supplement 1

NATIONAL AERONAUTICS AND SPACE ADMINISTRATION

APOLLO 14 MISSION REPORT

SUPPLEMENT 1

APOLLO 14 GUIDANCE, NAVIGATION, AND CONTROL SYSTEMS PERFORMANCE ANALYSIS REPORT

DISTRIBUTION AND REFERENCING

This paper is not suitable for general distribution or referencing. It may be referenced only in other working correspondence and documents by participating organizations.

MANNED SPACECRAFT CENTER
HOUSTON, TEXAS
JANUARY 1972

MSC-04112
Supplement 1

APOLLO 14 MISSION REPORT

SUPPLEMENT 1

APOLLO 14 GUIDANCE, NAVIGATION, AND CONTROL SYSTEMS PERFORMANCE ANALYSIS REPORT

PREPARED BY

TRW Systems

APPROVED BY

James A. McDivitt
Colonel, USAF
Manager, Apollo Spacecraft Program

NATIONAL AERONAUTICS AND SPACE ADMINISTRATION
MANNED SPACECRAFT CENTER
HOUSTON, TEXAS
January 1972

PROJECT TECHNICAL REPORT

TASK E-38D

APOLLO 14 GUIDANCE, NAVIGATION AND CONTROL SYSTEMS PERFORMANCE ANALYSIS REPORT

NAS 9-8166

28 JUNE 1971

Prepared for
NATIONAL AERONAUTICS AND SPACE ADMINISTRATION
MANNED SPACECRAFT CENTER
HOUSTON, TEXAS

Prepared by
Guidance and Control Systems Department

TRW
SYSTEMS GROUP

PROJECT TECHNICAL REPORT

TASK E-38D

APOLLO 14 GUIDANCE, NAVIGATION AND CONTROL SYSTEMS PERFORMANCE ANALYSIS REPORT

NAS 9-8166

28 JUNE 1971

Prepared for
NATIONAL AERONAUTICS AND SPACE ADMINISTRATION
MANNED SPACECRAFT CENTER
HOUSTON, TEXAS

Prepared by
Guidance and Control Systems Department

Approved by J. E. Alexander

J. E. Alexander, Manager
Guidance & Control Systems
Department

TRW
SYSTEMS GROUP

TABLE OF CONTENTS

ILLUSTRATIONS

NOMENCLATURE

ACA	Attitude controller assembly
ACB (X, Y, Z)	Accelerometer bias (channels X, Y, Z)
ADSRA (S, Y, Z)	Gyro drift due to acceleration along the spin reference axis (channels X, Y, Z)
ADIA (X, Y, Z)	Gyro drift due to acceleration along the input axis (channels X, Y, Z)
AEA	Abort electronics assembly
AET	Apollo elapsed time
AGS	Abort guidance system
AOT	Alignment optical telescope
APS	Ascent propulsion system
ASA	Abort sensor assembly
BDA	Bermuda (tracking station)
CDU	Coupling data unit
COAS	Crew optical alignment sight
CM	Command module
CMC	Command module computer
CSM	Command and service module
DAP	Digital auto pilot
DEDA	Data entry and display assembly
DPS	Descent propulsion system
DSKY	Display and keyboard
EPC	Earth prelaunch calibration
FDAI	Flight director attitude indicator
FTP	Full throttle point
GDA	Gimbal drive actuator
GDS	Goldstone (tracking station)
GET	Ground elapsed time (range time)
G&N	Guidance and navigation
GSOP	Guidance system operational plan
GTS	Gimbal trim system
HOPE	Houston operations predictor/estimator
IFC	Inflight calibration
IMU	Inertial measurement unit

IRIG	Inertial rate integrating gyro
JPL	Jet Propulsion Laboratory
LGC	LM guidance computer
LM	Lunar module
LOS	Line-of-sight
LOX	Liquid oxygen
LR	Landing radar
Luminary ID	Lunar module computer program for Apollo 14
MCC	Midcourse correction
MERU	Milli-earth rotational units
MIC	Minimum impulse control (mode)
MSC	Manned Spacecraft Center
NASA	National Aeronautics and Space Administration
NAT	NASA Apollo trajectory
Omega P' error	Rate error about P axis
Omega U' error	Rate error about U' axis
Omega V' error	Rate error about V' axis
PDI	Powered descent initiation
P error	Yaw axis error
PGNCS	Primary guidance, navigation and control system
PIC	Pre-installation calibration
PIPA	Pulsed, integrating pendulous accelerometer
PPM	Parts per million
PTC	Passive thermal control
RCS	Reaction control system
REFSMMAT	Reference to stable member matrix
RHC	Rotational hand controller
RMS	Root mean square
RR	Rendezvous radar
RSS	Root of the sum of the squares
RTCC	Real time control center
S/C	Spacecraft
$\widehat{\text{Sec}}$	Arc seconds
SFE (X, Y, Z)	Scale factor (channels X, Y, Z)

NOMENCLATURE (Concluded)

SM	Service module
SODB	System operational data book
SPS	Service propulsion system
SIVBIU	Saturn IVB instrumentation unit
SXT	Sextant
TEI	Trans-earth insertion
THC	Translational hand controller
TIG	Time of ignition
TLI	Trans-lunar injection
TTCA	Thrust and translation controller
U error	Computed errors
U' error	Computed errors
V error	Computed errors
V' error	Computed errors
VG	Velocity gained
VO (X, Y, Z)	Velocity offset (X, Y, Z)
a_X	Measured gravity vector in IMU coordinates (X)
a_Y	Measured gravity vector in IMU coordinates (Y)
a_Z	Measured gravity vector in IMU coordinates (Z)
μg	Micro-gravities
P, U, V axis	DAP control axis oriented relative to LM body axes as shown below:

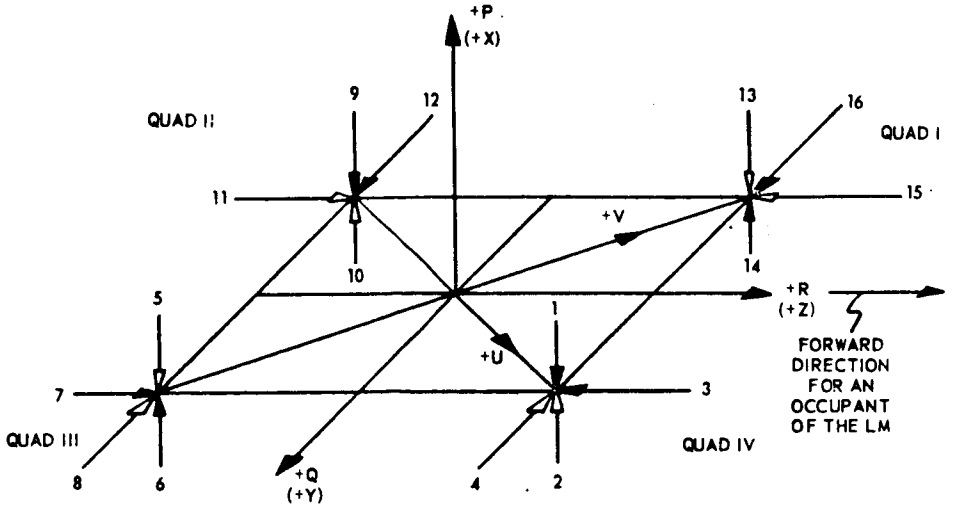

1.1 INTRODUCTION

1.1 General

This report concludes the analysis of the inflight performance of the Apollo 14 mission guidance, navigation and control equipment onboard the lunar module. The analyses supplement those presented in the Apollo 14 Mission Report (reference 1). This document was prepared and submitted under MSC/TRW Task E-38D, "Guidance and Control Requirements and Evaluation."

2.0 SUMMARY

The Guidance, Navigation and Control Systems installed in the Apollo 14 spacecraft performed as expected with three exceptions. In the CSM, a light on the entry monitor system malfunctioned and in the LM, the AGS computer down-moded to standby during the final phases of rendezvous and a crack appeared in a glass window of the AGS data entry and display assembly. In addition during powered descent the landing radar locked up in an unusual manner. These anomalies are fully explained in the MSC Mission Report (Reference 1).

This report contains the results of additional studies which were conducted to confirm the conclusions of the MSC Mission Report and contains analyses which were not completed in time to meet the Mission Report deadline.

The LM IMU data were examined during the lunar descent phase for the purpose of estimating the system errors present. No anomalous error build-up was detected and system errors observed can be easily accounted for using platform and instrument misalignments which are well within the system uncertainty.

AGS sensor data were examined in detail during coasting and powered flight. A higher than normal change in drift rate on one of the gyros was detected during the mission which prompted a detailed examination of the other instruments. Available data revealed no anomalous behavior from the other instruments and the observed performance compared favorably with preflight estimates and previous mission data. Cause for the large change in drift rate on the one gyro is unknown.

During the two automatic controlled periods (P63 and P64) of powered descent a marked reduction in RCS fuel consumption was observed as compared with previous lunar landings. Incomplete knowledge of RCS consumption effects due to software changes incorporated in Apollo 14 prompted a study of the observation to determine the underlying cause or causes. Detailed analysis appears to indicate that the software

changes had only secondary effects and the primary causes were differences in the RCS/GTS/slosh interaction for Apollo 14 during P63 and fewer redesignates, less manual inputs and a smaller pitchover maneuver for Apollo 14 during P64.

An anomaly in the landing radar subsystem during the first part of lunar descent caused some distortion of the LGC update information. Detailed analysis of the update telemetry data indicates actual update to the LGC altitude at the time of lock-on was approximately 870 ft.

3.0 LM IMU PERFORMANCE

For the best estimate descent trajectory, LM IMU acceleration data were integrated from an initial RTCC vector prior to start of ullage to time of touchdown. In order to null the lunar surface relative velocities in all directions after touchdown, the following LM IMU errors were assumed:

Error Source	Error Arc Sec	Ratio Error/1σ
Platform misalignment about Y (ϕ_y)	-57	0.28
Z accelerometer misalignment toward X (ZXMSL)	-43	2.1
Y accelerometer misalignment toward Z (YZMSL)	-10	0.5

As shown, the error sources are well within the 3σ design uncertainty and are consistent with errors recovered on previous missions.

Utilizing the corrected LM IMU data, reconstructed touchdown coordinates compare favorably with the post-mission best estimate coordinates as derived from P20 SXT tracking, P22 RR tracking and lunar surface alignments.

	Latitude (Deg)	Longitude (Deg)	Radius (ft)
Reconstructed	-3.650	-17.489	5697110
Best Estimate Post-mission	-3.674	-17.478	5696826

LM IMU PIPA biases were stable throughout the periods of LM activity and required no inflight updating. A history of biases is shown in Table 3.1. The only set of biases which differ significantly from the others were those measured shortly after IMU powerup on the lunar surface. A continuous monitoring of the instruments in this time period indicates the biases require at least one hour to settle in on their pre-shutdown bias levels.

TABLE 3.1

LM PIPA BIAS MEASUREMENTS (CM/SEC^2)

	Prelaunch [1] Mean	Pre-PDI 107:47 AET	Post Touchdown 108:20 AET	Post-Powerup on Lunar Surface 130:08 AET	Pre-Lunar Liftoff 140:51 AET	Post Ascent 142:03 AET
X	1.27	1.27	1.27	1.55	1.36	1.36
Y	1.63	1.62	1.66	1.89	1.76	1.71
Z	1.39	1.39	1.39	1.56	1.33	1.45

[1] Compensation load values were:

X = 1.30 cm/sec^2

Y = 1.65 cm/sec^2

Z = 1.39 cm/sec^2

4.0 AGS ASA PERFORMANCE

4.1 Gyro Errors

4.1.1 Free Flight Performance

Gyro bias drift was measured four times during the mission using the onboard calibration programs and in addition, differences between AGS determined body attitude and PGNCS determined body attitude were computed at various other times from postflight data. The divergence rate in the AGS and PGNCS body attitude comparisons was interpreted as AGS gyro drift. Table 4.1 presents the gyro drift histories for Apollo 14.

The X gyro bias was well behaved throughout the mission with observed fluctuations easily within design limits and well within the range of performance observed on previous missions. The Y gyro bias was somewhat noisier than usual; in particular the 0.23°/hr shift between the inflight calibrations. The second inflight calibration was possibly degraded due to higher than allowable vehicle rates or CDU switching transients. Since the calibration was conducted on the backside of the moon, data are not available to determine the cause. For subsequent missions, new procedures have been recommended for inflight calibrations which should assure validity of the calibration data.

A definite problem existed in the Z gyro, first evidenced by a large shift between the prelaunch data and the first inflight calibration. The gyro bias shift did, however, remain within fail limits but the bias value continued to grow and never did stabilize. A thorough investigation by the ASA manufacturer failed to uncover a cause for the gyro problem. A survey of historical data on the ASA electronics and gyro itself provided no clues as to which part of the gyro loop should be suspected. Due to the inability to isolate the cause no correction action is being considered.

4.1.2 Powered Flight Performance

AGS and PGNCS body attitude comparisons were run for both descent and ascent and are shown in Figures 4-1 through 4-6. Because of the noise associated with the differences, primarily the result of the 40 arc second granularity assoicated with PGNCS gimbal angles and interpolation noise induced by sizable LM body rates, the differences were smoothed by using a 40 second moving third order polynominal fit. Even with the substantial smoothing, the two axes with the highest amplitude limit cycle, Y and Z, exhibit considerable fluctuations and noise during the burn phases. With reasonable confidence however, quantitative judgements can be made about the gyros from the plots. An average total drift is recoverable from the data by measuring the change in angular error between ignition and cutoff. The difference between the average total drift during the burn and residual drift observed either prior to the burn or after cutoff is considered the dynamic drift in this analysis. In addition, known vehicle maneuvers executed during the burn help isolate various system errors.

In reviewing Figure 4-1, a definite step change in the X direction occurs at the time the vehicle pitches over upon entrance to the approach phase program (P64). If the PGNCS system is assumed a perfect reference, such a step change would be caused by AGS attitude misalignment, X gyro input axis misalignment or a combination of both. Since the observed X axis step would result if the Z axis attitude reference were misaligned by 325 arc seconds (based on the size of the pitch maneuver) and the Z axis channel actually shows an AGS attitude misalignment of approximately 400 arc seconds existing at the time of the maneuver, it can be concluded that the X error is primarily the result of Z axis attitude reference misalignment. The remaining 75 arc seconds can easily be attributed to uncertainty in the data and cannot be positively associated with any single error source.

A smaller step change is also reflected in the Z axis at the entrance to P64 (Figure 4-3) and is due to a misalignment of the attitude reference about the X axis.

For the descent comparisons (Figures 4-1 through 4-3) the average total drifts through the powered phase have been designated on the plots by a dashed line. Shown below are the drift values leading to a dynamic drift estimate.

Gyro	(A) Residual Static Drift Measured Pre-PDI*	(B) Total Drift Measured During Burn	Average Dynamic Drift (B-A)
X	0.10°/hr	0.49°/hr	0.39°/hr
Y	0.12°/hr	0.25°/hr	0.13°/hr
Z	0.29°/hr	0.73°/hr	0.44°/hr

A summary of all the recovered gyro errors estimated for descent are shown in Table 4.2 along with the preflight estimates for these errors. All are easily within the 3σ preflight estimate except the Z gyro error. As previously discussed, the Z gyro bias was unstable and continued to grow during descent. The growth in the static bias between ignition and touchdown is inseparable from the dynamic drift, but was definitely present and unrealistically increased the size of the dynamic error estimate.

For the ascent comparisons (Figures 4-4 through 4-6) again the average total drifts through the powered phase have been designated on the plots by a dashed line. The pulse exhibited in the X axis trace shortly after liftoff is the result of a timing error in the data and a high X axis body rate which existed for the duration of the pulse. The body rate, determined from DAP data, was at an average value of -.135°/sec for approximately 20 seconds. Based on the size of the error developed during that period, an estimated timing error of 36 ms was calculated. Analysis of the LGC and AEA clock values at the same time revealed a K-factor error of 30 ms. A K-factor error of 50 ms or greater is required before an update is considered. Velocity comparison data substantiated the timing error. The low frequency oscillation most evident in Y and Z and to a lesser degree in X during the ascent burn are probably the result of imperfect syncronization between the two data sources and a low frequency modulation on the body rate limit cycle. Because of the difference in DAP control axes(U' and V') and LM body axes and because of different limit cycles on each control axis an expected growing and shrinking of the

*Table 4.1 Column (5) minus column (4)

body rate amplitudes occurs. If a timing error exists, the attitude difference plots will be most severely affected when the body rates are the highest causing the apparent growing and then retreating to the steady state error. Shown below are the drift values leading to an estimate of the dynamic drift for the ascent burn.

Gyro	(A) Residual Static * Drift Measured Post Ascent	(B) Total Drift Measured During Ascent	Average Dynamic Drift (B-A)
X	.07	0.12	.05
Y	.01	-0.19	-.20
Z	.08	0.13	.05

A summary of all the recovered gyro errors estimated for ascent are shown in Table 4.2 along with the preflight estimates for these errors. All are easily within the 3σ preflight estimates.

*Table 4.1 Column (8) Minus Column (7)

Table 4.1. ASA 021 Gyro Bias Drift History

	(1) Preflight Mean	(2) First Inflight Calibration 103:25 AET	(3) Rev. 12 104:54 AET	(4) Second Inflight Calibration 103:54 AET	(5) Pre-PDI 107:49 AET	(6) Lunar Surface Calibration # 1 108:31 AET	(7) Lunar Surface Calibration # 2 141:11 AET	(8) Post Ascent 141:55 AET
X	0.11°/hr	0.06	0.18	0.07	0.17	0.09	0.09	0.16
Y	0.04°/hr	0.23	0.08	0	0.12	0.08	0.16	0.17
Z	0.60°/hr	1.87	2.03	1.61	1.90	2.04	2.25	2.33

Table 4.2 Gyro Bias Error Summary (deg/hr)

		Descent		
		ASA 021 Preflight Estimate		ASA 021 Inflight Estimate
		Mean	3σ	
Gyro fixed drift	X	0	0.45	0.10
	Y	0	0.46	0.12
	Z	0	0.46	0.29
X gyro spin axis mass unbalance		0	0.21	0.39*
Gyro dynamic drift	X	0.02	0.29	
	Y	0.12	0.30	0.13
	Z	0.12	0.31	0.44
Total (deg/hr)	X	0.02	0.57	0.49
	Y	0.12	0.55	0.25
	Z	0.12	0.56	0.73

		Ascent		
		ASA 021 Preflight Estimate		ASA 021 Inflight Estimate
		Mean	3σ	
Gyro fixed drift	X	0	0.42	.07
	Y	0	0.41	.01
	Z	0	0.41	.08
X gyro spin axis mass unbalance		0	0.64	0.05*
Gyro dynamic drift	X	0.02	0.26	
	Y	0.10	0.30	-0.20
	Z	0.10	0.37	0.05
Total (deg/hr)	X	0.02	0.88	0.12
	Y	0.10	0.54	-0.19
	Z	0.10	0.63	0.13

*Postflight data is not sufficient to separate X gyro spin axis mass unbalance and X gyro dynamic drift.

4.2 Accelerometer Errors

4.2.1 Free Flight Bias Stability

AGS accelerometer biases determined throughout the mission are presented in the table below and show acceptable long and short term stability.

	Preflight Data Mean	Docked IFC 103:25 AET	Undocked IFC 104:54 AET	Rev. 14 Pre PDI 107:44 AET	Rev. 31 Post Insertion 142:02 AET
X	356 μg	311	311	275	193
Y	49 μg	0	31	23	19
Z	- 20 μg	- 62	- 62	- 61	-105

4.2.2 LM Descent Velocity Comparisons

Sensed velocity residuals (in body coordinates) between AGS and corrected PGNCS measurements are shown in Figures 4-7 through 4-9. The sign of the residuals is defined by

$$\Delta V = V_{AGS} - V_{PGNCS}.$$

PGNCS sensed velocity increments were transformed to body coordinates and summed at a one second rate in order to form a baseline for AGS comparison. PGNCS CDU angles were used for the transformation so that ΔV is not dependent on either AGS or PGNCS gyro errors. Due to poor data quality the comparisons were terminated at PDI plus 424 seconds (108:09:30 AET). The sudden steps in the ΔV_x residual curve at full throttle point (108:02:52 AET) and at throttle recovery (108:08:47 AET) are the result of a timing error in the data of approximately 60 ms. In order to arrive at a set of instrument errors which reasonably explain the residual curves, it is useful to examine the correlation coefficients for the error terms in the AGS model. The AGS accelerometer modeled error terms are defined in Table 4.3. The following correlation matrix was generated from a nominal covariance matrix derived from the AGS Performance and Interface Specification.

Table 4.3. LM AGS Error Model (Accelerometer)

Mnemonic	Description
XAB	X accelerometer bias
YAB	Y accelerometer bias
ZAB	Z accelerometer bias
XASF	X accelerometer scale factor
XAMTY	X accelerometer misalignment toward Y
XAMTZ	X accelerometer misalignment toward Z
YAMTX	Y accelerometer misalignment toward X
YASF	Y accelerometer scale factor
YAMTZ	Y accelerometer misalignment toward Z
ZAMTX	Z accelerometer misalignment toward X
ZAMTY	Z accelerometer misalignment toward Y
ZASF	Z accelerometer scale factor
TB	Accelerometer timing bias

Matrix of AGS Error Correlation Coefficients
LM Descent Trajectory

XAB	YAB	ZAB	XASF	YAMTX	ZAMTX	TB	
1	0	0	-.98	0	0	-.21	XAB
	1	0	0	-.99	0	0	YAB
		1	0	0	-.99	0	ZAB
			1	0	0	.11	XASF
				1	0	0	YAMTX
					1	0	ZAMTX
						1	TB

Correlation coefficients vary between "-1 and +1," and are indicators of the interdependence of solution parameters. As a correlation coefficient approaches ± 1, the associated interrelationship of two parameters becomes most pronounced; as it approaches zero, the mutual influence vanishes.

The following conclusions are evident after inspection of the above matrix.

1) Dynamic bias and scale factor for the X-accelerometer cannot be separated but timing error is separable from these effects.

2) Dynamic bias and Y misalignment toward X are inseparable.

3) Dynamic bias and Z misalignment toward X are inseparable.

The method of grouping inseparable errors is somewhat arbitrary. In the table below X-accelerometer static bias, dynamic bias, and scale factor have been grouped into XAB; Y and Z-accelerometer dynamic bias and sensing axis misalignment have been grouped into YAMTX and ZAMTX respectively. The error magnitudes shown are the result of a weighted least squares fit of state errors to the velocity residual data. The static biases YAB and ZAB were determined from free flight data prior to PDI and were fixed in the solution.

Recovered Error Terms for Descent	Description	Error Magnitude
XAB[1]	X accelerometer Dynamic bias and scale factor error	-32 μg
YAB	Y accelerometer static bias	-18.7 μg
ZAB	Z accelerometer static bias	0.9 μg
YAMTX	Y accelerometer misalignment toward X and Y accelerometer dynamic bias	34 $\widehat{\text{sec}}$
ZAMTX	Z accelerometer misalignment toward X and Z accelerometer dynamic bias	- 70 $\widehat{\text{sec}}$
TB	Timing error	-0.06 sec

Note [1]: In addition, static bias of -36.4 μg determined from pre-PDI free flight data was included in the solution.

Velocity residual statistics after the least squares fit are indicators of the goodness of the fit. The difference between the standard deviation and the measurement noise estimate is an indicator of the effects of unmodeled errors (including residual PGNCS errors). The principal sources of measurement noise were investigated and predicted to be as follows:

	RMS Error-ft/sec
AGS Quantization	$.06/\sqrt{3}$
PGNCS Quantization	$.03/\sqrt{3}$
Interpolation Noise	Insignificant

The velocity residual statistics below indicate the actual measurement noise was within the predicted and a reasonable fit to the AGS modeled errors was accomplished.

Measurement Channel	Standard Deviation ft/sec	Measurement Noise Estimate ft/sec
X	.05	.02
Y	.06	.02
Z	.13	.02

4.2.3 Ascent Velocity Comparisons

Sensed velocity residuals (in body coordinates) between AGS and corrected PGNCS are shown in Figure 4-10 through 4-12. CDU angles were used to rotate PGNCS sensed velocity increments into body coordinates so that the AGS-PGNCS ΔV residuals are not dependent on gyro drift errors.

Examination of the residual plots after orbit insertion (141:52:54 AET) indicates no static accelerometer bias for the Y or Z instruments. A small bias error of -35 μg was indicated for the X instrument. The sudden step in the ΔV_x curve at insertion indicates a small timing error.

The residual curves during powered flight are due principally to dynamic and/or sensing axis misalignment errors. Again, insight into which terms in the AGS error model should be examined is gained from inspection of the correlation coefficients so a correlation matrix was derived in a manner similar to that described for descent. The correlation matrix is as follows:

Matrix of AGS Error Correlation Coefficients
LM Ascent Trajectory

XAB	YAB	ZAB	XASF	YAMTX	ZAMTX	TB	
1	0	0	-.96	0	0	.23	XAB
	1	0	0	-.98	0	0	YAB
		1	0	0	-.81	0	ZAB
			1	0	0	-.14	XASF
				1	0	0	YAMTX
					1	0	ZAMTX
						1	TB

The same conclusions arrived at for descent as to separable and inseparable errors are valid for ascent. As for descent a somewhat arbitrary grouping of the inseparable errors was chosen and is reflected in the table below. The error magnitudes obtained are the result of a weighted least squares fit of state errors to the velocity residual data.

Recovered Error Terms for Ascent	Description	Error Magnitude
XAB[1]	X accelerometer dynamic bias and scale factor error	-88 μg
YAMTX	Y accelerometer misalignment toward X and Y accelerometer dynamic bias	40 $\widehat{sec}$
ZAMTX	Z accelerometer misalignment toward X and Z accelerometer dynamic bias	-112 $\widehat{sec}$
TB	Timing error	-0.03 sec

Note [1]: In addition, static bias of -35 μg determined from post insertion data was included in the solution.

Velocity residual statistics after the least squares fit are quite good as evidenced in the following table.

Measurement Channel	Standard Deviation ft/sec	Measurement Noise Estimate ft/sec
X	.28	.08
Y	.12	.05
Z	.32	.06

The difference between the sample standard deviation and the measurement noise estimate is a measure of the effects of unmodeled errors.

4.2.4 Comparison to Preflight Performance Estimates

Since individual error terms for each accelerometer are not fully separable, it is necessary to derive a single performance index from the premission performance estimate to allow comparison with the in-flight results. This performance index represents a composite of static and dynamic errors and sensing axes misalignments. In order to combine the terms, all the non-bias errors were converted to equivalent acceleration errors and expressed in terms of μg. (Note: This is possible only because the ratios of the partials for the errors mentioned above are fairly constant through the descent and ascent trajectories. This fact

is also the reason for the high data correlation between these errors.) Premission performance estimates for ASA-021 are shown in Table 4.4 and 4.5 along with the AGS recovered errors, converted to equivalent μg, from the descent and ascent velocity comparisons. All the inflight errors are within the 3σ preflight estimates indicating normal behavior of the accelerometer instruments during powered flight.

Table 4.4 Descent Equivalent Accelerometer Bias Errors (μg)

Axis	Error Source	ASA-021 Inflight Estimate	ASA-021 Preflight Estimate Mean	ASA-021 Preflight Estimate 3σ
X	Bias, nonlinearity and dynamic errors		-25	102
	Scale factor		16	72
	Total	-123	- 9	126
Y	Bias, nonlinearity and dynamic errors		-10	87
	Internal sensing axis alignment		38	36
	ASA alignment to navigation base*		0	195
	Total	63	28	216
Z	Bias, nonlinearity and dynamic errors		6	87
	Internal sensing axis alignment		-24	12
	ASA alignment to navigation base*		0	195
	Total	-175	-18	213

*Value taken from LM AGS capability estimate.

Table 4.5 Ascent Equivalent Accelerometer Bias Errors (μg)

Axis	Error Source	ASA-021 Inflight Estimate	ASA-021 Preflight Estimate Mean	ASA-021 Preflight Estimate 3σ
X	Bias, nonlinearity and dynamic errors		-25	102
	Scale factor		12	54
	Total	-68	-13	114
Y	Bias, nonlinearity and dynamic errors		-10	87
	Internal Sensing Axis alignment		30	30
	ASA alignment to navigation base *		0	156
	Total	24	20	180
Z	Bias, nonlinearity and dynamic errors		6	87
	Internal sensing axis alignment		-19	9
	ASA alignment to navigation base *		0	156
	Total	-88	-13	180

*Value taken from LM AGS capability estimate.

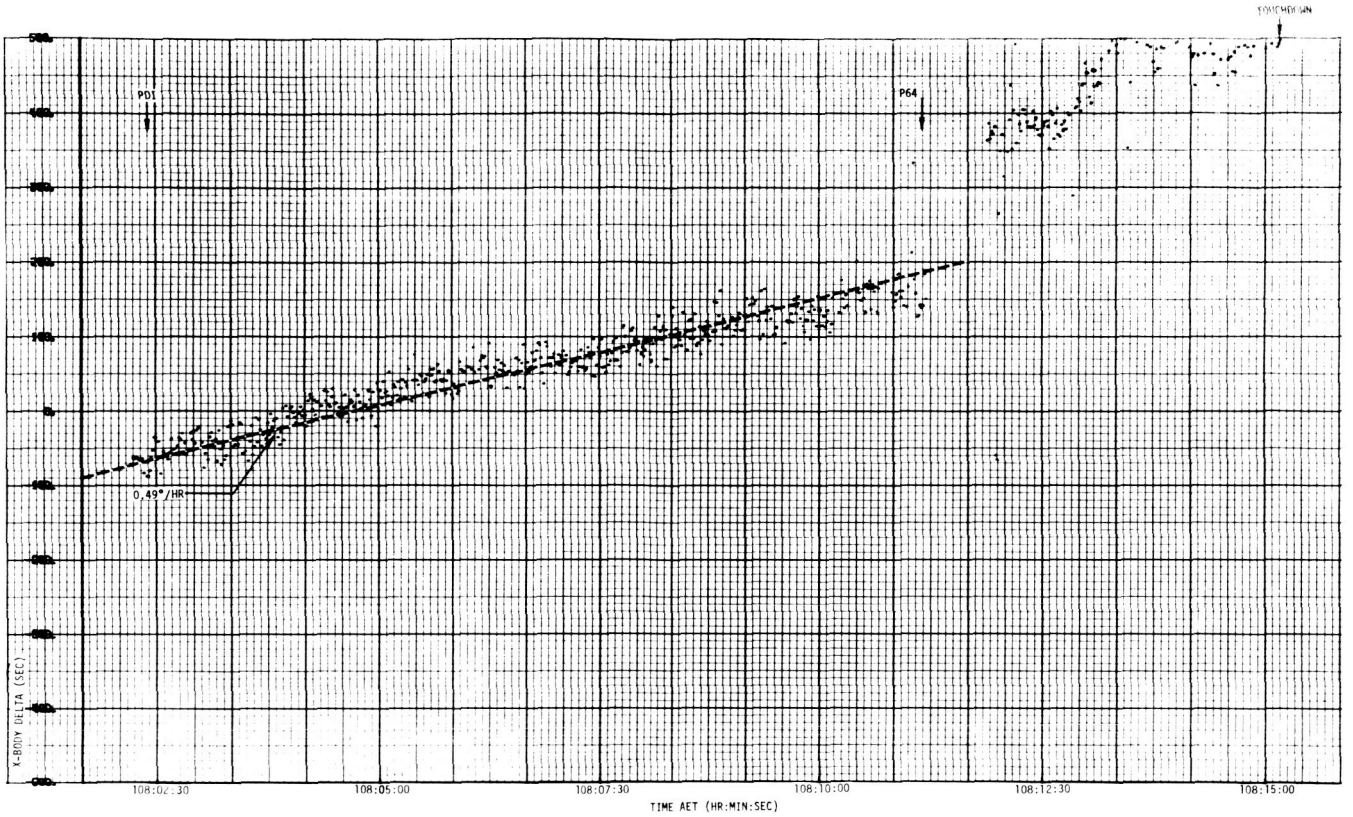

Figure 4-1 AGS Minus PGNCS Body Angle Difference

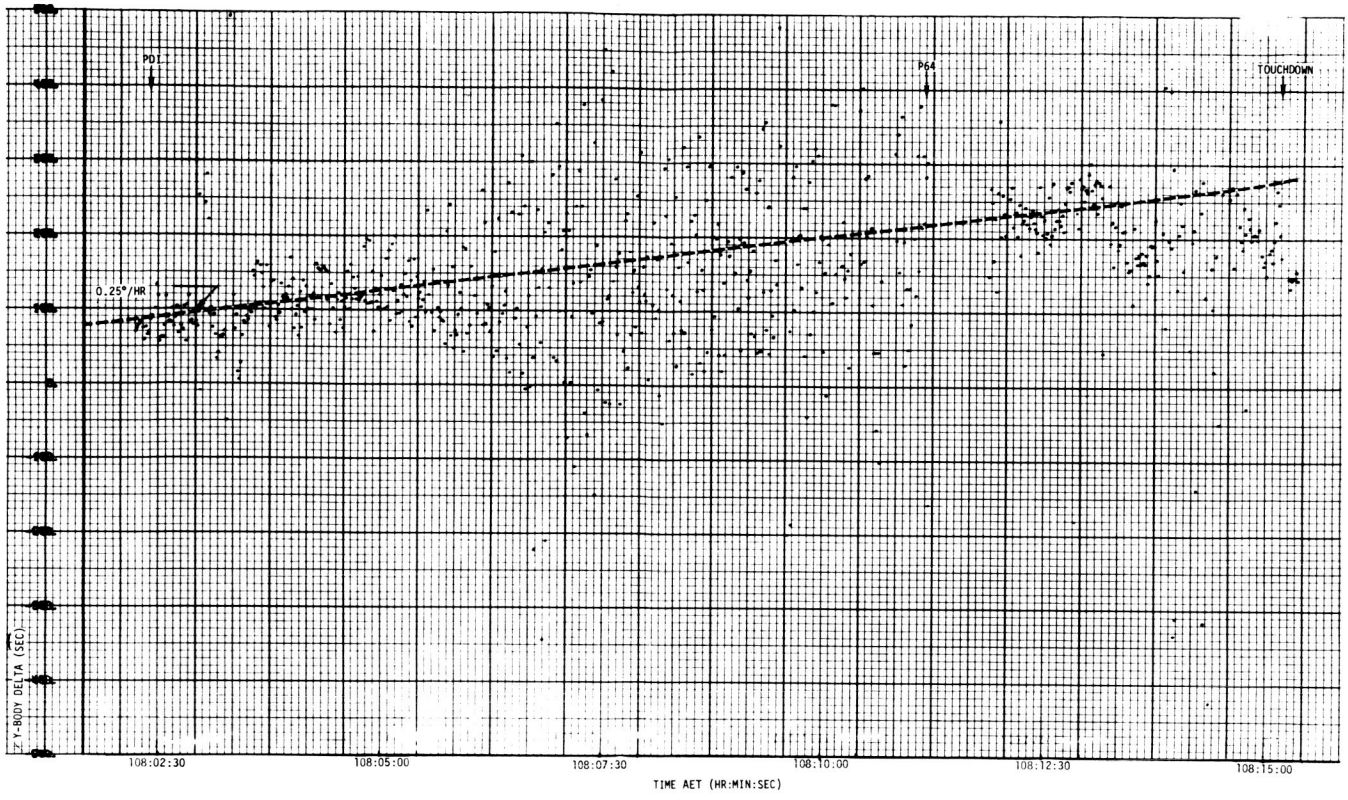

Figure 4-2 AGS Minus PGNCS Body Angle Difference

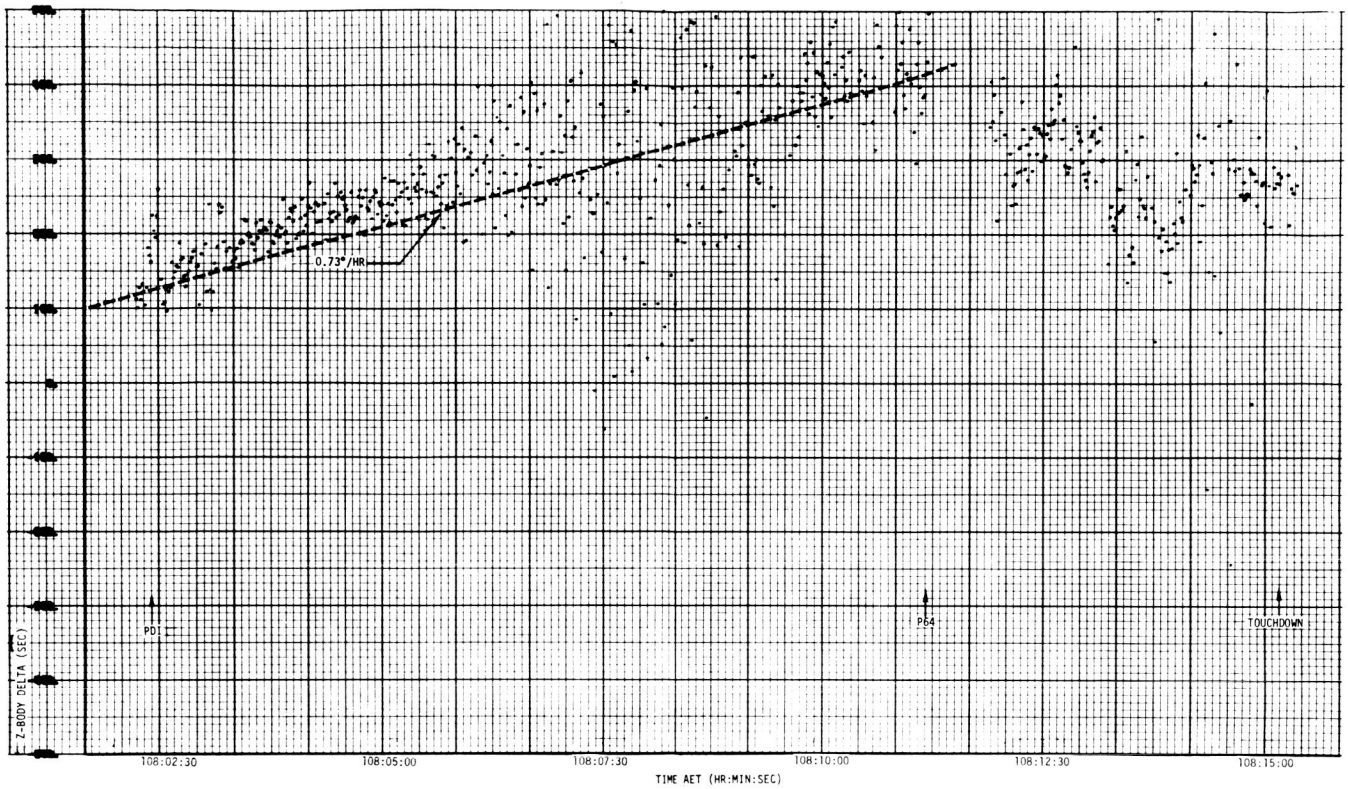

Figure 4-3 AGS Minus PGNCS Body Angle Difference

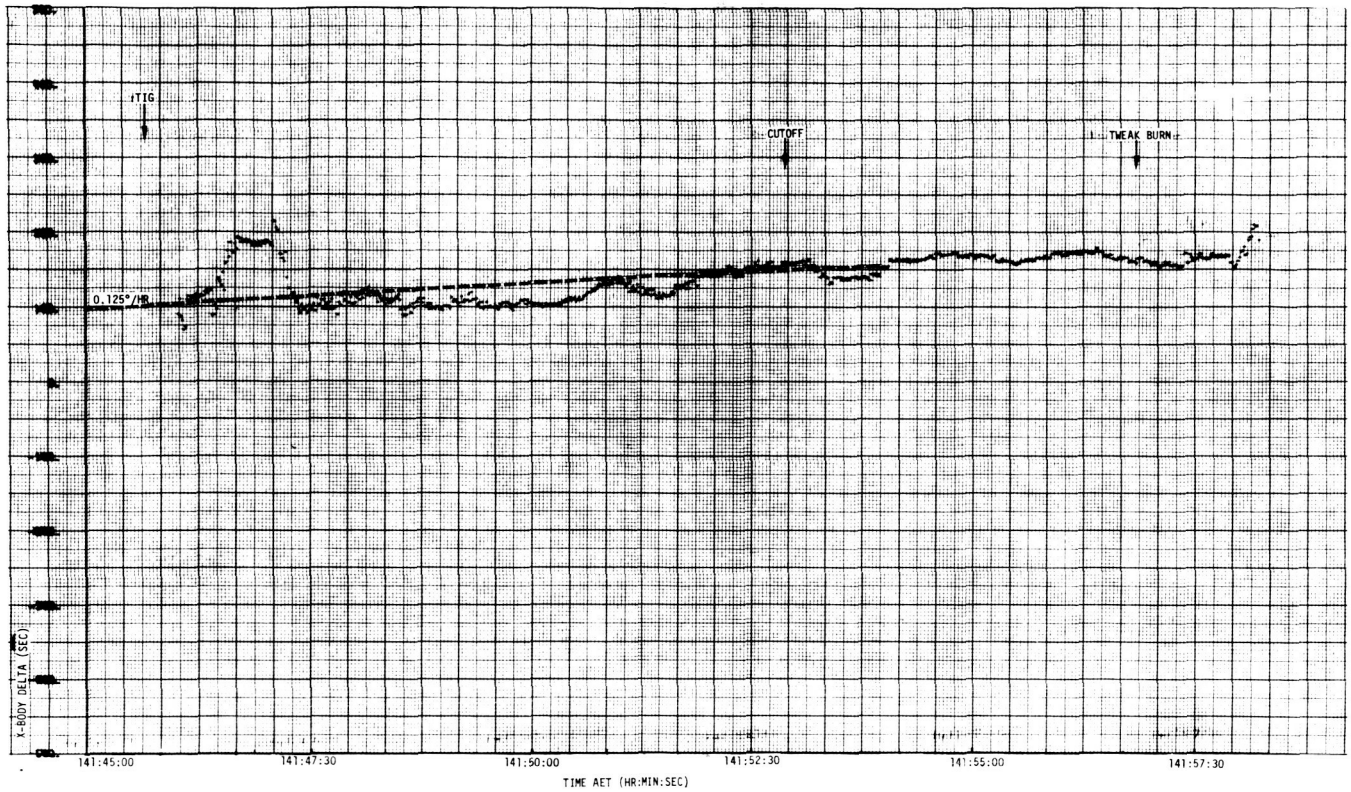

Figure 4-4 AGS Minus PGNCS Body Angle Difference

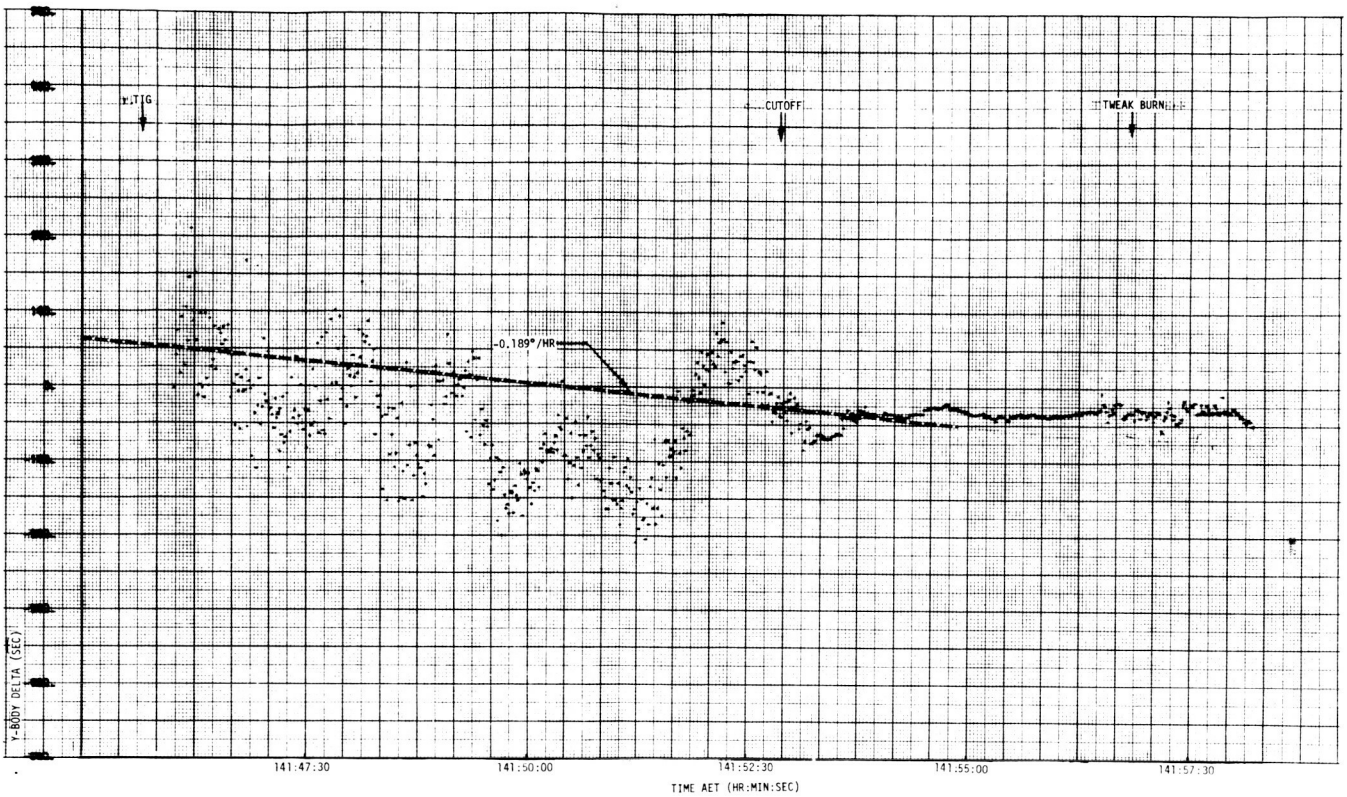

Figure 4-5 AGS Minus PGNCS Body Angle Difference

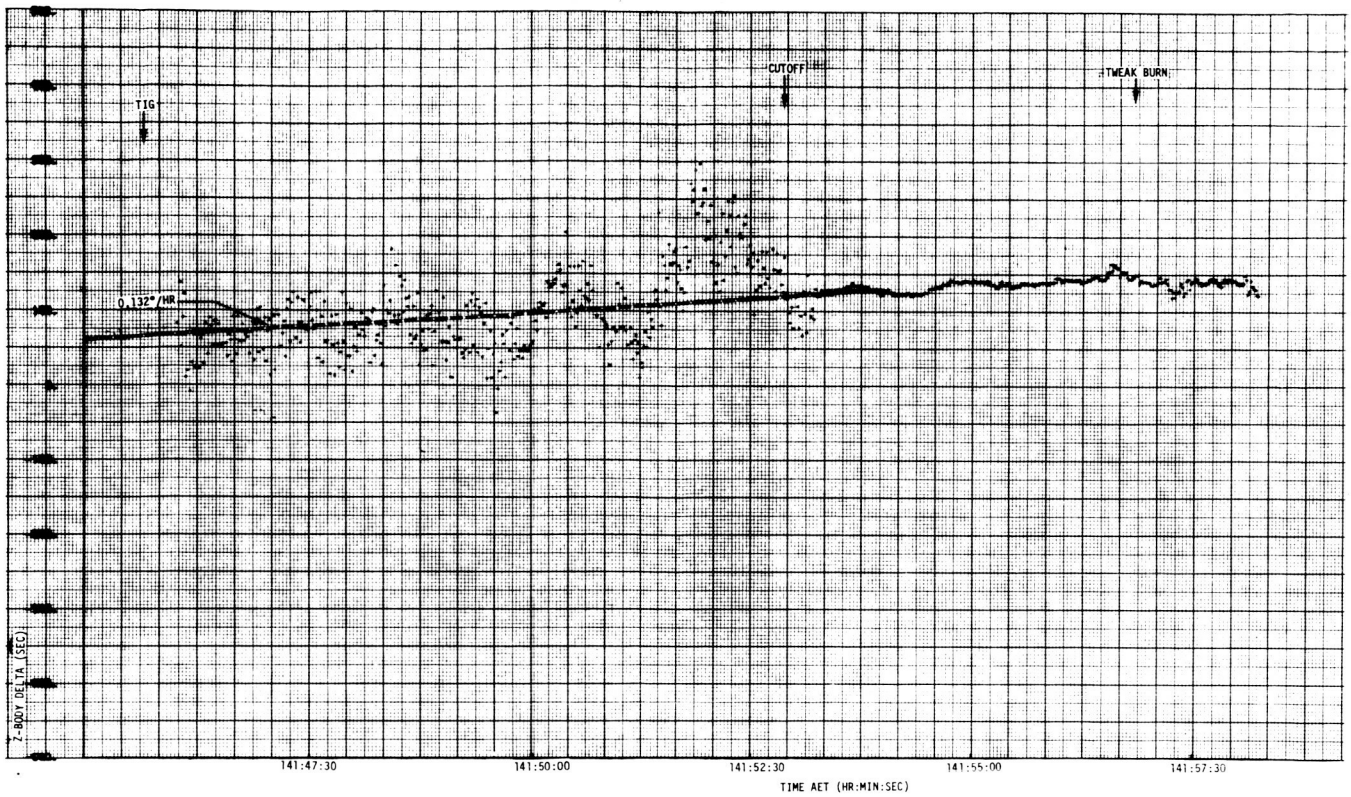

Figure 4-6 AGS Minus PGNCS Body Angle Difference

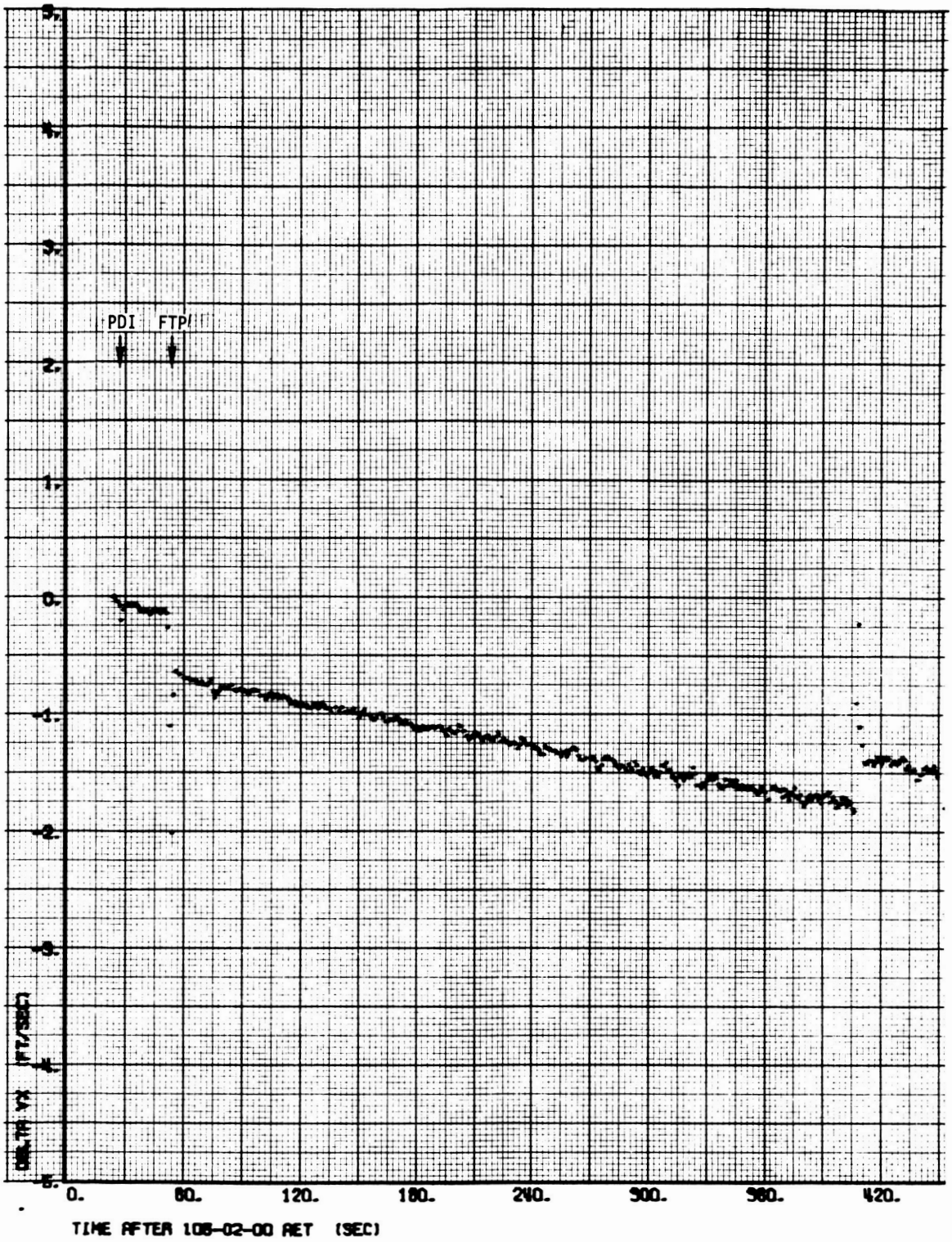

Figure 4-7 Apollo 14 AGS-PGNCS Velocity Residuals (LM Descent)

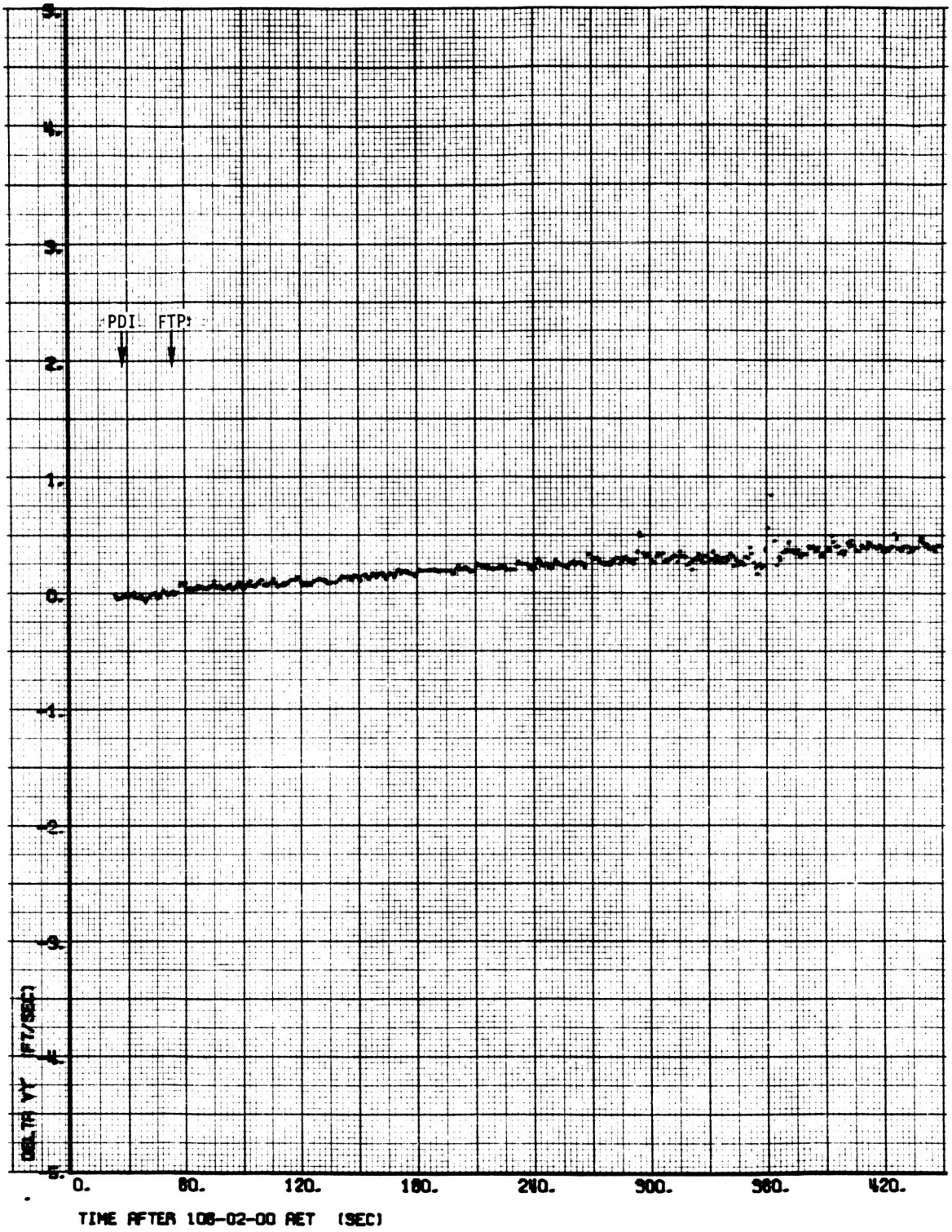

Figure 4-8 Apollo 14 AGS-PGNCS Velocity Residuals (LM Descent)

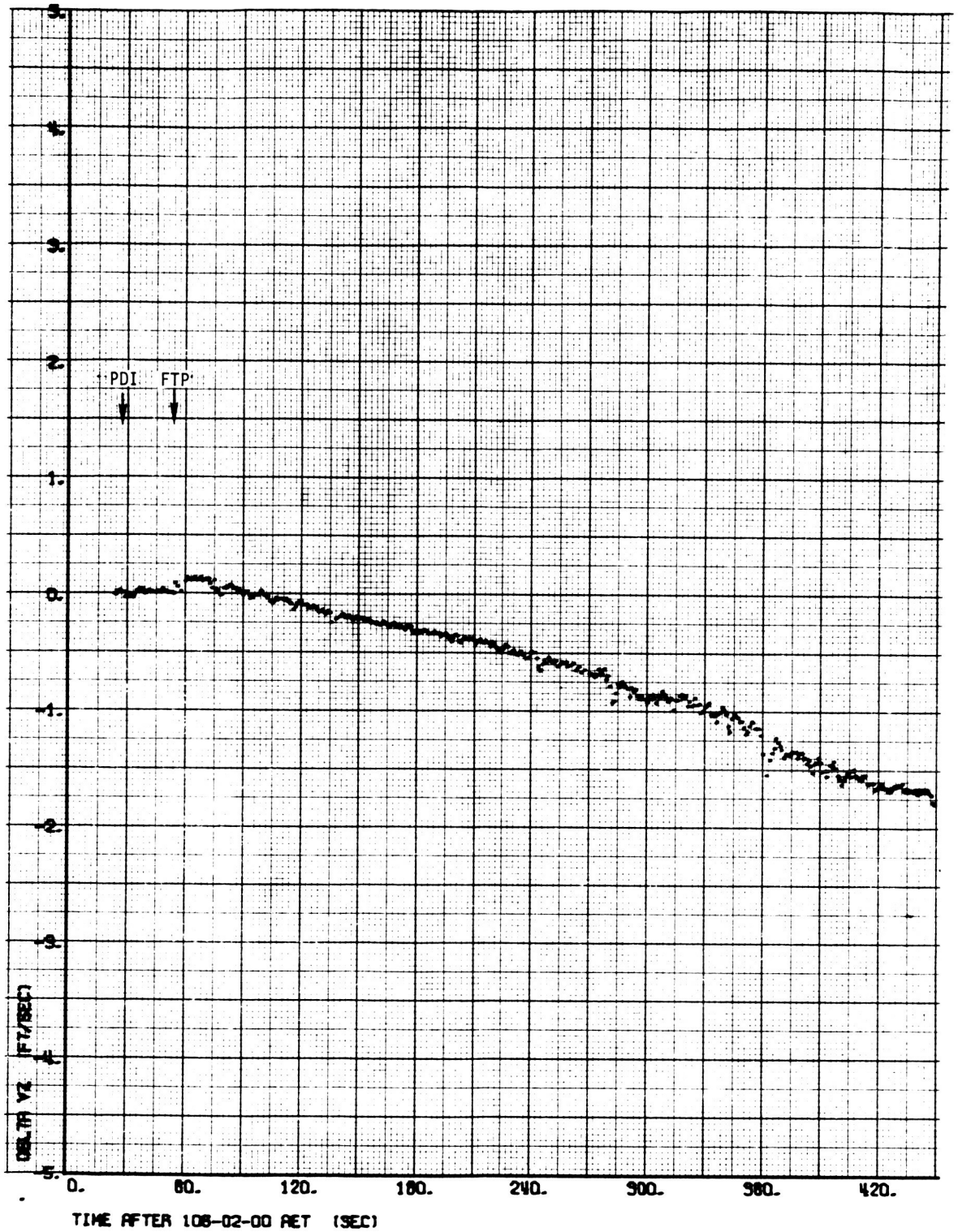

Figure 4-9 Apollo 14 AGS-PGNCS Velocity Residuals (LM Descent)

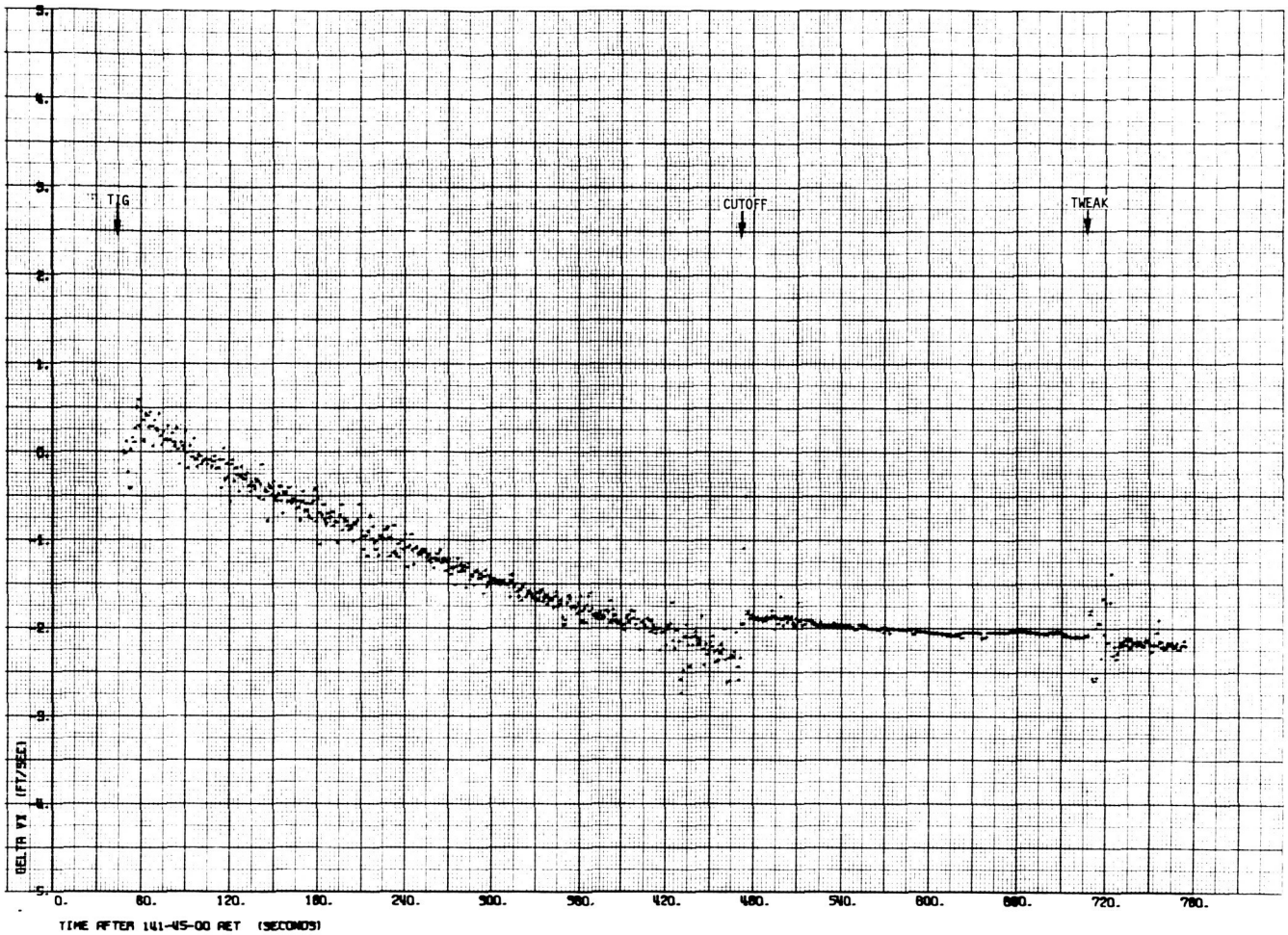

Figure 4-10 Apollo 14 AGS-PGNCS Velocity Residuals (LM Ascent)

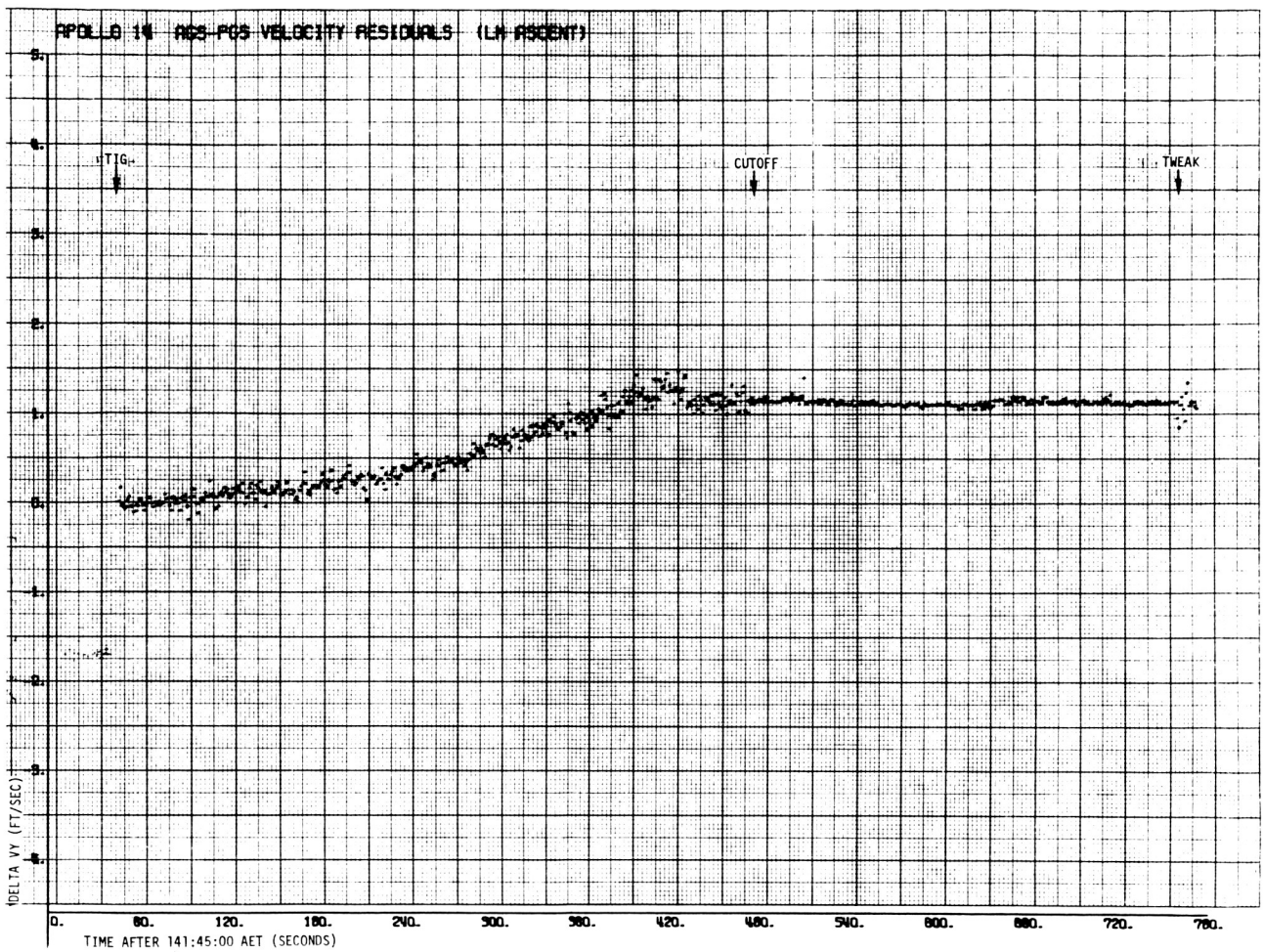

Figure 4-11 Apollo 14 AGS-PGNCS Velocity Residuals (LM Ascent)

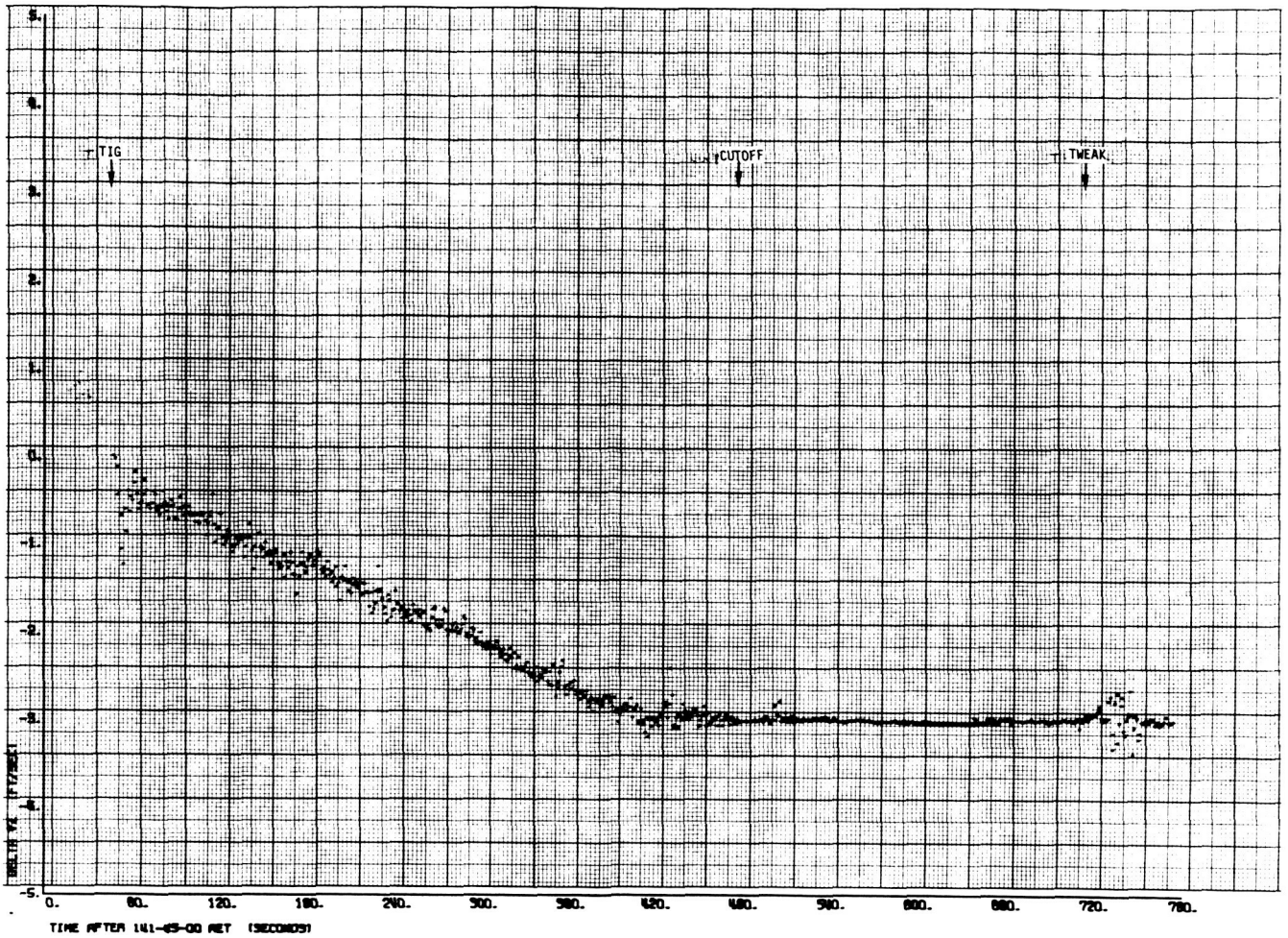

Figure 4-12 Apollo 14 AGS-PGNCS Velocity Residuals (LM Ascent)

5.0 LM DIGITAL AUTOPILOT

The Luminary ID (Rev. 5) Digital Autopilot was implemented in the LM Guidance Computer for the Apollo 14 mission. Detailed analyses of the powered descent and ascent were performed and are summarized below.

Descent

The sequencing through the lunar descent programs was nominal and the time durations of each phase of descent compared well with the Apollo 12 descent. Slosh activity became evident in P63 approximately 270 seconds into the descent burn, which corresponded well with the behavior in previous lunar descents. The Apollo 14 slosh frequency was slightly less than that observed in previous missions. The RCS propellant usage during P63 and P64 for Apollo 14 (14.89 lbs) was approximately half of the amount used in the Apollo 12 mission (32.01 lbs) and is explained as follows:

P63 - The total RCS propellant consumption during P63 was 7.06 lbs. This is low in comparison with 15.66 lbs for Apollo 12. A plot of RCS propellant consumption during powered descent is given in Figure 5-1. A comparison of the RCS propellant consumption per axis during P63 in Apollo 12 and 14 indicates that a major portion of the total reduction in Apollo 14 lies in U' axis. Of the total reduction of 8.60 lbs, the breakdown is: 6.54 lbs in U' axis, 2.00 lbs in V' axis, and 0.06 lbs in P axis. The attitude error and rate error in Apollo 12 and 14 in the U' axis were compared to verify this. Figures 5-2 and 5-3 show the plots for a corresponding representative period of 3 minutes in P63 for Apollo 12 and 14, respectively. The maximum peak-to-peak rate excursion is 3.8 deg/sec for Apollo 12, and 1.6 deg/sec for Apollo 14. Although the attitude error plots cannot easily be correlated, the rate error plots substantiate the reduction in RCS propellant consumption in U' axis.

Detailed analysis indicates the lower RCS propellant consumption during P63 on Apollo 14 was a direct result of reduced slosh frequency instability in the Gimbal Trim System Control. Slosh amplitudes were about one-half as large as those on Apollo 12 at corresponding times-from-PDI. Although the slosh activity became dominant at approximately the same time for the Apollo 12 and 14 missions, RCS/slosh interaction began two minutes later on Apollo 14 in both pitch and roll. The DAP estimated pitch rates were plotted during the period when RCS/slosh interaction began on Apollo 12 and compared with the corresponding period starting at PDI + 4 minutes for Apollo 14. The peak pitch rates computed by the DAP were almost as large on Apollo 14 but the composition of the signals was different. The Apollo 12 peak rates were composed of 50% to 90% slosh. The Apollo 14 peak rates were only 30% to 50% slosh induced. The slosh diverged very rapidly during this period of the Apollo 12 flight, but on Apollo 14 the slosh did not diverge and the majority of RCS firings were in response to steady state rates. Because of the lower slosh component in the DAP rates, the RCS jet firings were of shorter duration on Apollo 14 and propellant was conserved. Cause for the reduced slosh was lower frequency response in the Gimbal Trim System. The Gimbal Trim System is stable at the low frequencies and will not allow a divergence unless the energy of the system is being diverted to the slosh. The above observations about the control signal indicate that the Apollo 14 engine actuator was unable to generate slosh divergence at the same rates as the Apollo 12 actuator. Actuator test data indicated the actuator drive rate was lower on Apollo 14 than Apollo 12. Therefore, a slower actuator response appears to be the underlying cause of reduced RCS propellant consumption during P63.

P64 - The total RCS propellant required for attitude control during P63 was 7.83 lbs as against 16.35 lbs for Apollo 12. Unlike that in P63, the reduction in the RCS propellant consumption is almost equally distributed in the three axis. A combination of the following causes accounts for the difference during P64:

a) There was significant activity in all axes near the end of P64 in Apollo 12 due to manual RHC commands which were not present in Apollo 14. This alone is estimated to account for about 20% of the reduction in RCS propellant consumption in P64 of Apollo 14.

b) There were five redesignations in Apollo 12 compared to one in Apollo 14. These five redesignates caused considerable jet firings in all axes. Yaw axes firings were most pronounced. It is estimated that the redesignations in Apollo 12 and the subsequently induced additional slosh activity account for about 50% of the reduced propellant consumption in P64 of Apollo 14.

c) The automatic pitchover maneuver in P64 caused greater change in pitch rate in Apollo 12 than in Apollo 14. (The maximum pitch rate in Apollo 12 was -12.1 deg/sec and that in Apollo 14 was -10.5 deg/sec). This and the subsequently induced additional slosh activity are estimated to account for about 30% of the reduction in propellant consumption.

The LM DAP performance during P66 defies exact comparison with previous missions because of the manual control mode and the individual pilots choice in landing techniques.

The conditions observed on the DSKY at the entrance to P66 were:

Horizontal Velocity:	34.5 fps
Altitude Rate:	-11.2 fps
Altitude:	281 ft.

The maximum estimated rates exclusive of the interval near touchdown were:

OMEGAP:	-4.25 deg/sec
OMEGAQ:	-7.08 deg/sec
OMEGAR:	4.05 deg/sec

At the time of touchdown, the estimated rates were:

OMEGAP:	-1.37 deg/sec
OMEGAQ:	-2.67 deg/sec
OMEGAR:	-1.27 deg/sec

These rates were much smaller than the corresponding ones in Apollo 12.

The total RCS propellant consumption for attitude control during P66 was 64.97 lbs. This compares with 60.25 lbs for Apollo 12.

A considerable thrust oscillation was observed during the landing phase in Apollo 11 and 12 missions. The main cause was identified as the failure to account for angular accelerations in the throttle command computation. In addition, the "descent engine lag" constant should have realistically been 0.08 sec instead of the previous value of 0.2 sec, and the gain in the throttle command computation routine was too high. All of the above problems were corrected in the flight software for Apollo 14 and the throttle commands during P66 revealed negligible oscillation. Thus, the LM DAP performance during P66 was nominal and in conformity with the preflight simulation results.

Powered Ascent

Lunar liftoff and lunar orbit insertion were accomplished during LGC Powered Ascent Program P12. The maximum attitude errors and rate errors near liftoff were:

PERROR:	-5.15 deg	OMEGAP ERROR:	2.61 deg/sec
U'ERROR:	7.30 deg	OMEGAU'ERROR:	-3.07 deg/sec
V'ERROR:	9.45 deg	OMEGAV'ERROR:	-3.02 deg/sec

The CDUY output indicated a pitchover of approximately 51.2 degrees and the pitchover maneuver lasted for 9 seconds. During this interval the maximum pitch rate was 13.21 deg/sec and the maximum angular acceleration was 6.77 deg/sec^2. This pitchover seems smoother than that in Apollo 12 in which the same maneuver was performed in 5 secs and with higher pitch rate and angular acceleration.

The ascent burn was performed with the APS interconnect open such that the RCS jets consumed APS propellant. About 71.80 lbs of APS propellant was used by the RCS jets for attitude control. This consumption was about 10 lbs higher than its preflight estimate. The reason was found to be a large roll moment offset. Taking this into consideration, the RCS propellant consumption was nominal. Thus, the LM DAP performance during powered ascent was found nominal and satisfactory.

FIGURE 5-1
RCS PROPELLANT CONSUMPTION DURING DESCENT

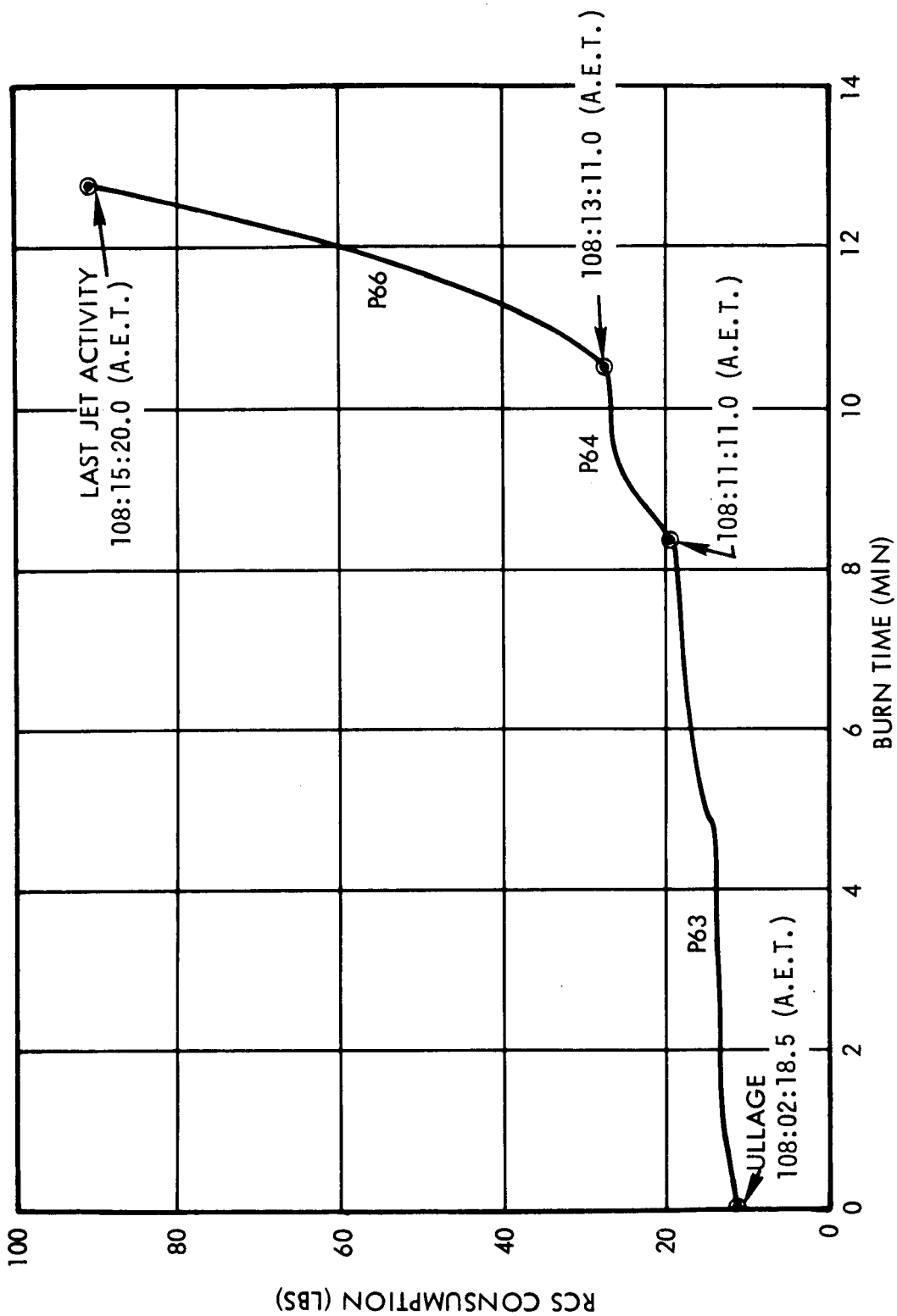

FIGURE 5-2

ATTITUDE AND RATE ERRORS DURING P63: U' AXIS, APOLLO 12

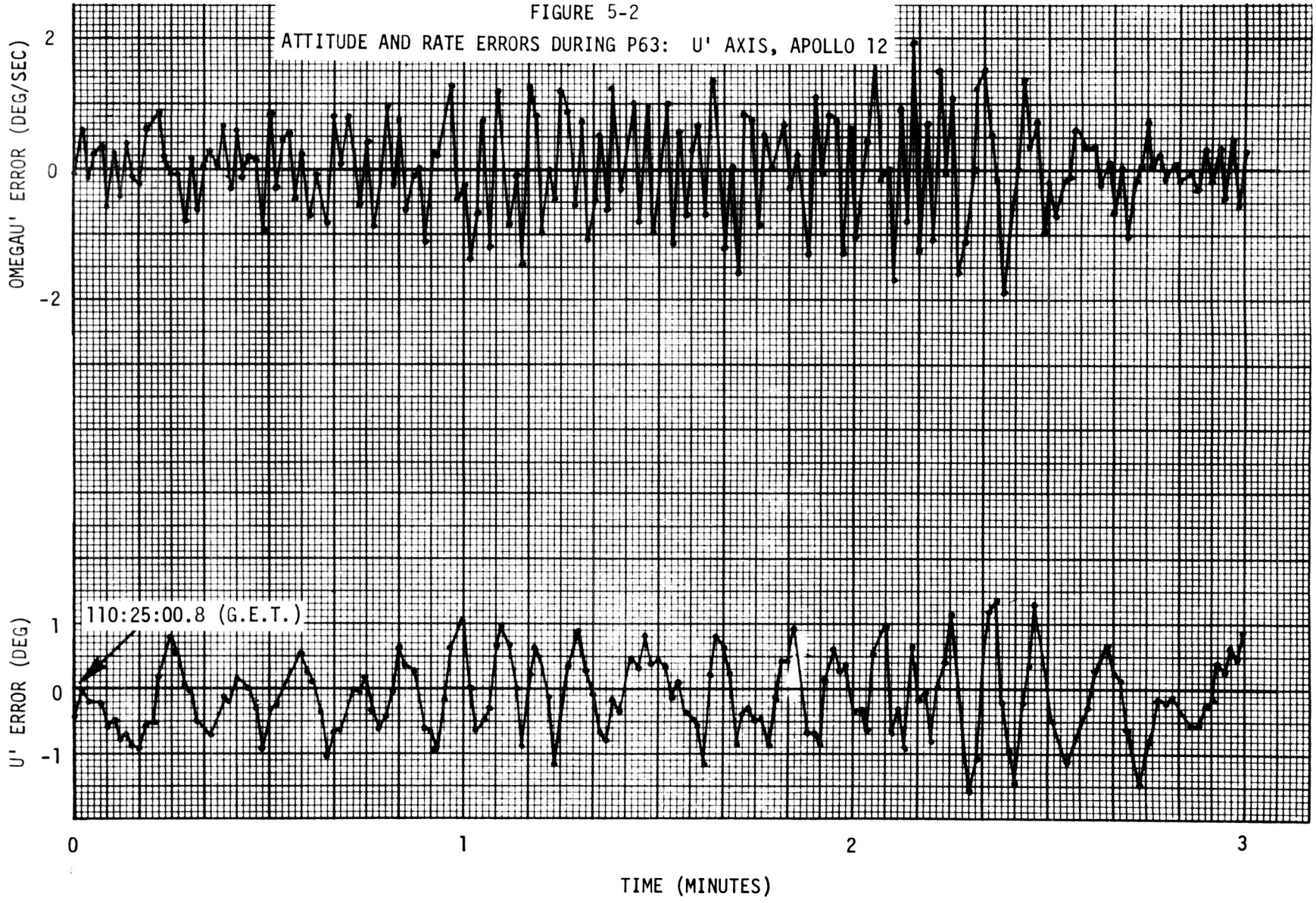

FIGURE 5-3

ATTITUDE AND RATE ERRORS DURING P63: U' AXIS, APOLLO 14

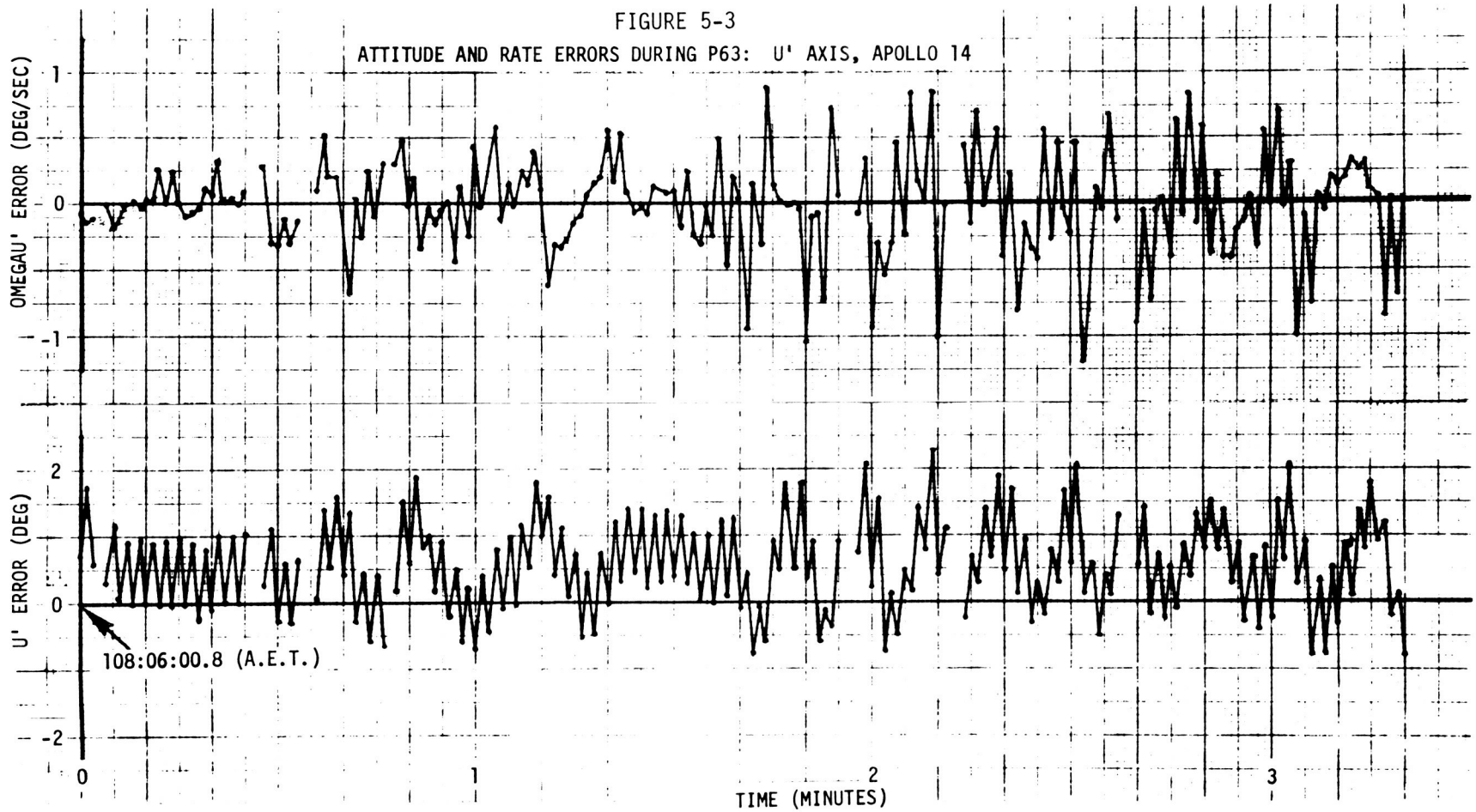

6.0 LGC UPDATING DURING DESCENT

6.1 Altitude Updating

The differences between the LR radar measured altitude and the LGC onboard estimate of altitude are shown in Figure 6-1. The large ΔH values (approximately 1000 ft) shown on the plot at lock-on do not represent state vector errors. The radar range beam took several seconds to settle in on a reasonable value and for that reason the first few ΔH values are invalid. The invalid data had no affect on the state vector since the astronaut did not allow updating until sometime between 108:09:27.5 AET (PDI plus 421 seconds) and 108:09:35.5 AET (PDI plus 429 seconds). Poor data communication during that interval precludes precise determination of the time for start of updating. If it is assumed the updating started mid-way between at 108:09:31.5 AET and if the proper weighting coefficients are applied to the ΔH data, a total altitude update of approximately 870 ft was applied to the onboard state vector before the ΔH diminished to zero at 108:10:0.5 AET (PDI plus 454 seconds). The onboard updating is similiarly reflected in a plot of altitude determined from onboard state vectors shown in Figure 6-2. At 108:09:31.5 AET when updating started the altitude plot shows a departure from its previously established trend reflecting a positive change in altitude and reflects an adjustment of the descent rate as the guidance steering returns the spacecraft to the desired descent trajectory.

6.2 Velocity Updating

Velocity updating is presented in Figures 6-3 through 6-5 and was computed by extracting gravity effects and accelerometer sensed thrust velocity from each state vector change between computer cycles. The residuals from such a solution yield the remaining input to the state during descent; landing radar updates. The only significant updating occurred immediately after radar lock-on. None of the channels appeared to exhibit heavy distributions of updates in any one direction which substantiates the good accuracy of the inertial data up to the start of radar updating. Through-out the period of radar updating the data were considerably quieter and

less active then observed on Apollo 12, which is significant in that the Apollo 14 radar data were considered noiser due to the rougher terrain that the LM passed over on Apollo 14. This confirms that the data goodness test being applied to incoming LR data by the LGC is smoothing the data and with minimal effect on real information contained in the signal, since LGC navigation errors at touchdown were less than 0.5 ft/sec. Differences between the LGC navigated moon relative state at the time of touchdown and the last landing radar velocities at touchdown are shown below:

	LGC Minus LR (Antenna Coordinates)
ΔV_x	0.01 ft/sec
ΔV_y	-0.47 ft/sec
ΔV_z	0.09 ft/sec

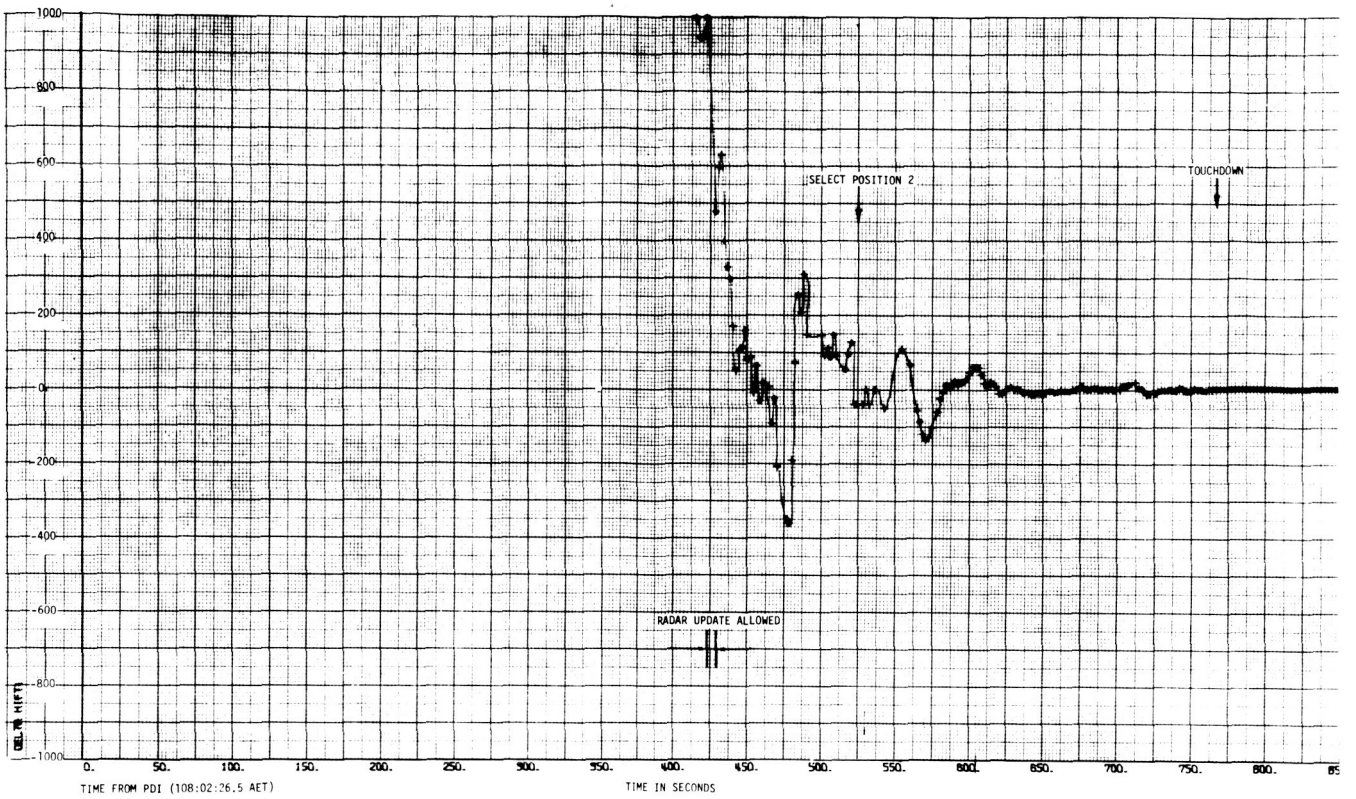

Figure 6-1 LR Altitude Minus LGC Altitude

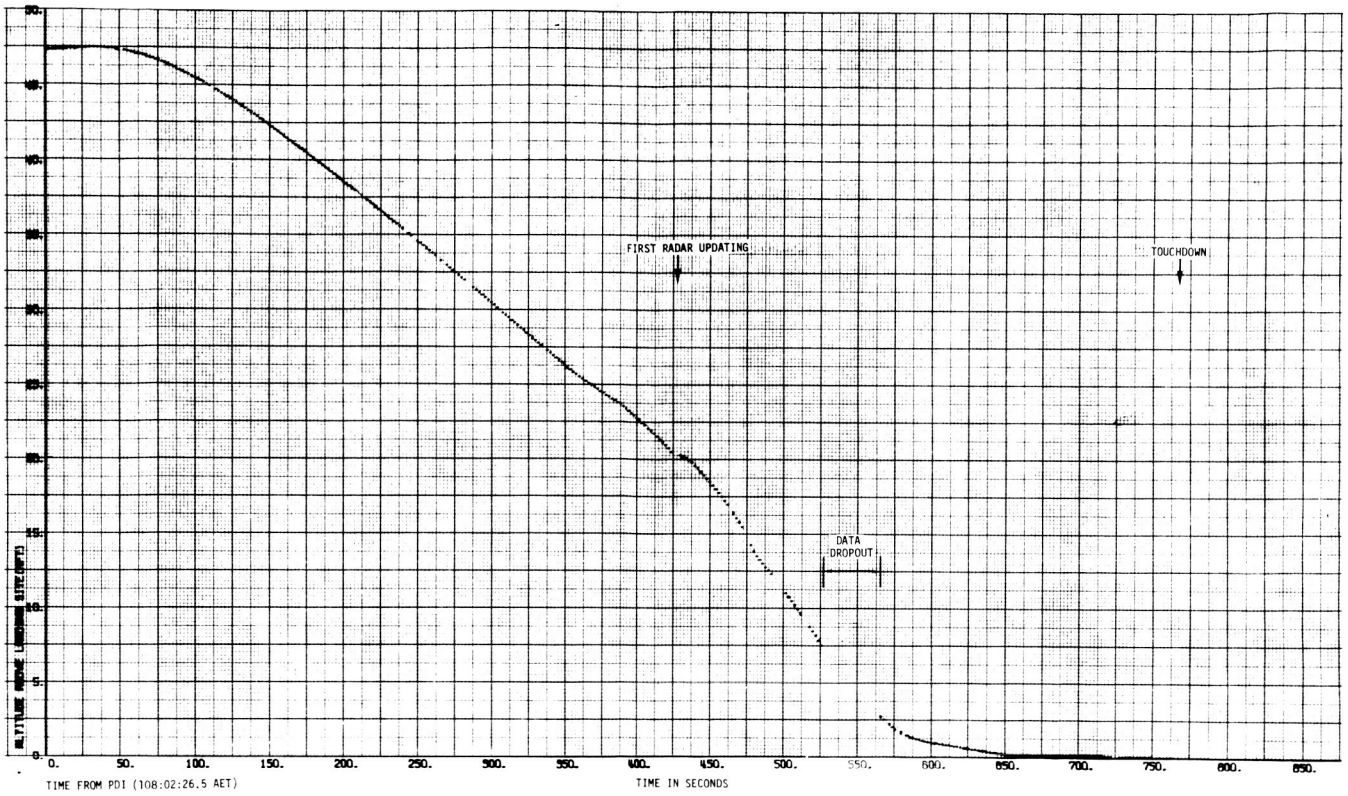

Figure 6-2 Altitude Above Landing Site

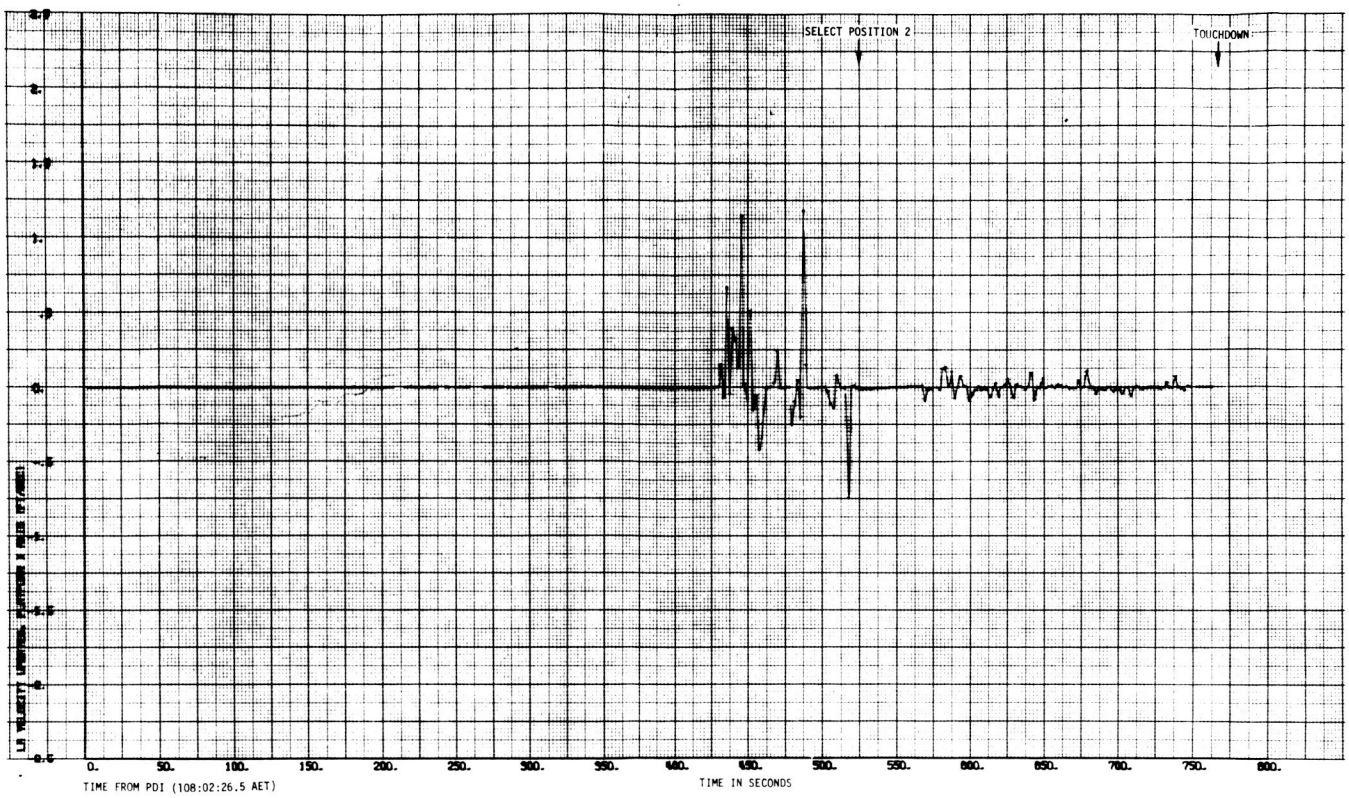

Figure 6-3 LR Velocity Updates, Platform X-Axis

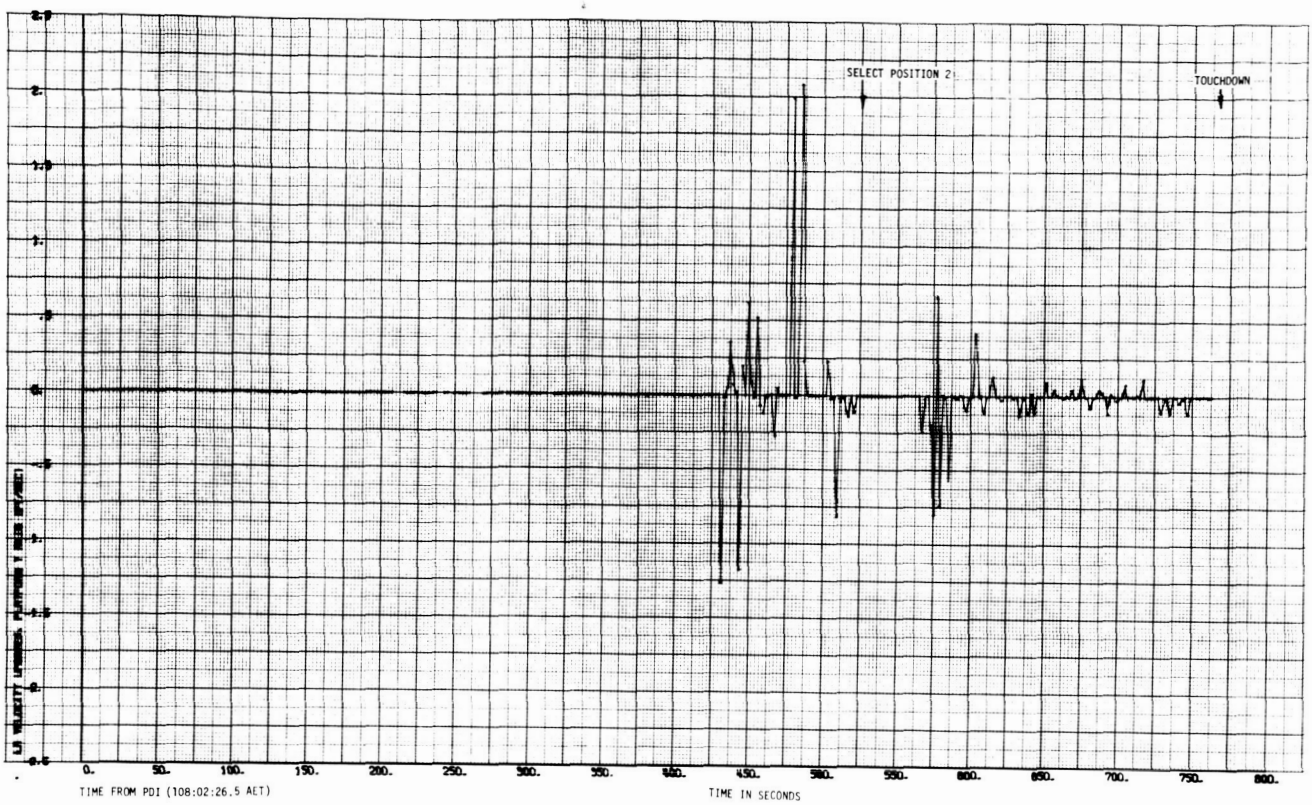

Figure 6-4 LR Velocity Updates, Platform Y-Axis

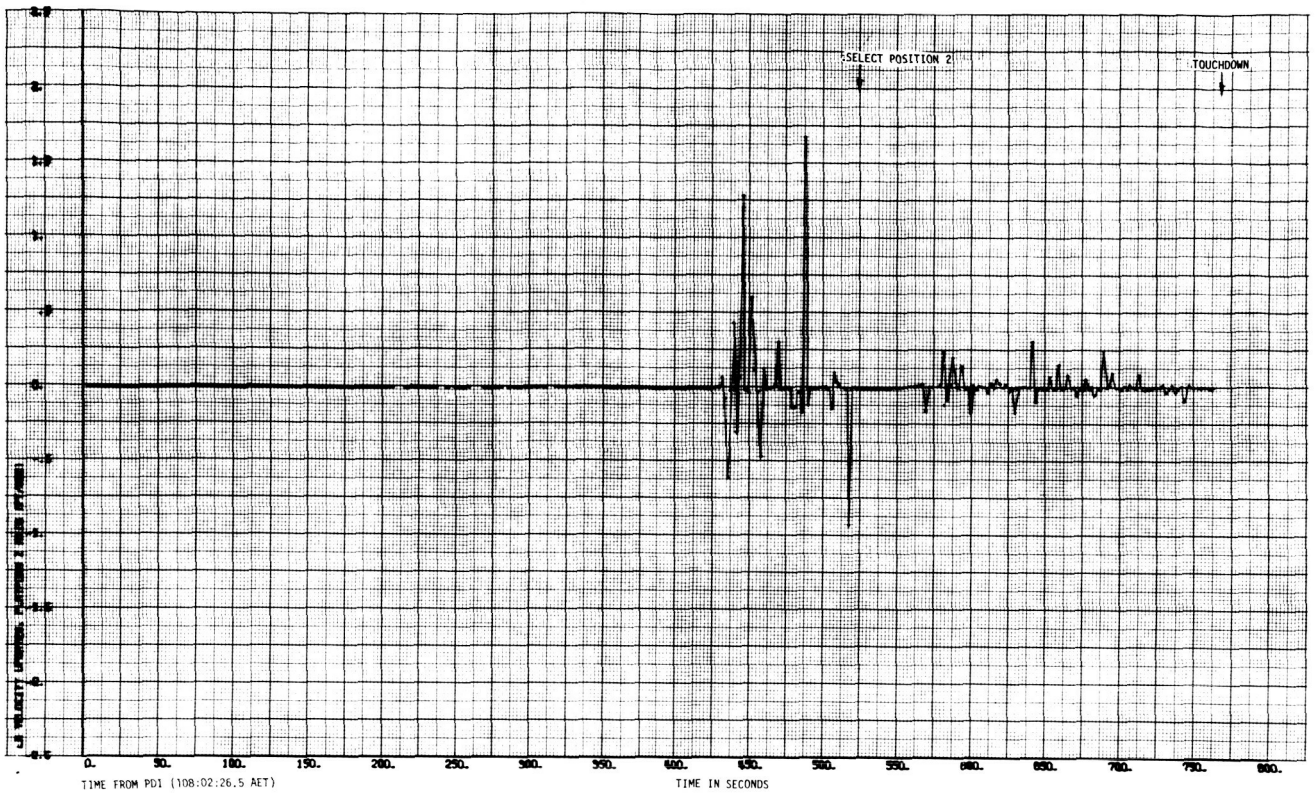

Figure 6-5 LR Velocity Updates, Platform Z-Axis

REFERENCES

1. MSC Report MSC-04112, "Apollo 14 Mission Report," dated May 1971.

☆ U.S. GOVERNMENT PRINTING OFFICE: 1972—779-262/421